Structure-function relationship of new peptides activating human Nav1.1

Ludivine Lopez, Stephan de Waard, Hervé Meudal, Cécile Caumes, Kuldip Khakh, Steve Peigneur, Barbara Oliveira-Mendes, Sophia Lin, Jolien de Waele, Jérôme Montnach, et al.

Biomedicine & Pharmacotherapy 165 (2023) 115173

Contents lists available at ScienceDirect

Biomedicine & Pharmacotherapy

journal homepage: www.elsevier.com/locate/biopha

Structure-function relationship of new peptides activating human $Na_v1.1$

Ludivine Lopez [a,b], Stephan De Waard [a,c], Hervé Meudal [d], Cécile Caumes [b], Kuldip Khakh [e], Steve Peigneur [f], Barbara Oliveira-Mendes [a], Sophia Lin [e], Jolien De Waele [g], Jérôme Montnach [a], Sandrine Cestèle [h], Agnès Tessier [a], J.P. Johnson [e], Massimo Mantegazza [h], Jan Tytgat [f], Charles Cohen [e], Rémy Béroud [b], Frank Bosmans [g], Céline Landon [d], Michel De Waard [a,b,c,*,1]

[a] Nantes Université, CNRS, INSERM, l'institut du thorax, F-44000 Nantes, France
[b] Smartox Biotechnology, Saint-Egrève, France
[c] LabEx "Ion Channels, Science and Therapeutics", Valbonne, France
[d] Center for Molecular Biophysics, CNRS, rue Charles Sadron, CS 80054, Orléans 45071, France
[e] Xenon Pharmaceuticals, Burnaby, British Columbia, Canada
[f] University of Leuven, 3000 Leuven, Belgium
[g] Department of Basic and Applied Medical Sciences, Ghent University, Ghent, Belgium
[h] Université Cote d'Azur, CNRS UMR 7275, Institute of Molecular and Cellular Pharmacology, Valbonne-Sophia Antipolis, France

ARTICLE INFO

Keywords:
Drug discovery
JzTx-34
Pharmacology
h$Na_v1.1$ channel
Biophysics
High-throughput screening
Automated patch clamp
Cellular assay
Peptide synthesis
Lead optimization
Structural functional relationships
Dravet disease

ABSTRACT

$Na_v1.1$ is an important pharmacological target as this voltage-gated sodium channel is involved in neurological and cardiac syndromes. Channel activators are actively sought to try to compensate for haploinsufficiency in several of these pathologies. Herein we used a natural source of new peptide compounds active on ion channels and screened for drugs capable to inhibit channel inactivation as a way to compensate for decreased channel function. We discovered that JzTx-34 is highly active on $Na_v1.1$ and subsequently performed a full structure-activity relationship investigation to identify its pharmacophore. These experiments will help interpret the mechanism of action of this and formerly identified peptides as well as the future identification of new peptides. We also reveal structural determinants that make natural ICK peptides active against $Na_v1.1$ challenging to synthesize. Altogether, the knowledge gained by this study will help facilitate the discovery and development of new compounds active on this critical ion channel target.

1. Introduction

Voltage-gated sodium channels (Na_v) are responsible for the initiation and propagation of action potentials (AP) in the central and peripheral nervous system. Of the nine subtypes that are expressed in humans (from $Na_v1.1$ to $Na_v1.9$), three are preferentially expressed in the central nervous system: $Na_v1.1$ encoded by the *SCN1A* gene, $Na_v1.2$ by *SCN2A* and $Na_v1.6$ by *SCN8A*. Neuronal expression of $Na_v1.3$ has also been reported, but appears to be regulated developmentally with low expression in adults. Owing to the recent divergence in gene family origin, the amino acid sequences of Na_v channels bear very important similarities. This is most striking for $Na_v1.1$ and $Na_v1.2$, for which sequence identity is 93 % in the 24 transmembrane segments and somewhat lower in the cytoplasmic regions. The homology is less for $Na_v1.6$ but remains high nevertheless. In spite of sequence identities, these channels localize differently in neuronal tissues implying a functional specialization for each of them.

$Na_v1.1$ differs from both $Na_v1.2$ and $Na_v1.6$ by being largely expressed in the AIS of inhibitory neurons, and particularly in parvalbumin-positive fast-spiking neurons [1,2], while $Na_v1.2$ and

Abbreviations: AD, Alzheimer disease; ASD, autism spectrum disorder; DEE, developmental and epileptic encephalopathy; DMEM, Dulbecco's Modified Eagle's Medium; DMF, dimethylformamide; DS, Dravet syndrome; GEFS+, genetic epilepsy with febrile Seizure plus; ICK, Inhibitor Cystine Knot; Na_v, voltage-gated sodium channels; SPPS, solid-phase peptide synthesis; SUDEP, sudden unexpected death in epilepsy; TANGO, Targeted Augmentation of Nuclear Gene Output.

* Corresponding author at: Nantes Université, CNRS, INSERM, l'institut du thorax, F-44000 Nantes, France.
E-mail address: michel.dewaard@univ-nantes.fr (M. De Waard).
[1] ORCID: 0000-0002-2782-961.

https://doi.org/10.1016/j.biopha.2023.115173
Received 23 March 2023; Received in revised form 11 July 2023; Accepted 12 July 2023
Available online 13 July 2023

$Na_v1.6$ are expressed predominantly in excitatory glutamatergic neurons. $Na_v1.1$ is thus expected to play significant roles in tuning down neuronal network excitability [3]. This was indeed confirmed by studies on GABAergic interneurons with loss-of-function mutations in the *SCN1A* gene illustrating reduced Na^+ current amplitudes [4] and spike amplitude decrement during AP burst, leading to decreased inhibitory circuit activity [2]. In agreement with the important physiological function of Na_v channels, mutations of the genes encoding $Na_v1.1$, $Na_v1.2$ and $Na_v1.6$ generate a myriad of severe neurological disorders. In the case of $Na_v1.1$, gain-of-function mutations have been linked to two neurological syndromes: familial hemiplegic migraine type 3, characterized by severe migraine with aura and transient hemiplegia [5], and a spectrum of epileptic phenotypes including extremely severe early onset developmental and epileptic encephalopathies [6–8]. Loss-of-function mutations of $Na_v1.1$ cause the severe developmental and epileptic encephalopathy (DEE) Dravet syndrome (DS) [9] and the milder genetic epilepsy with febrile Seizure plus (GEFS+) spectrum [10]. DS results from *SCN1A* haploinsufficiency [11]. The incidence of this pathology in the US population is about one out of 20,000 [12]. Patients affected by DS experience early-onset spontaneous tonic-clonic seizures, often in response to elevated body temperature, and develop cognitive and motor disabilities in parallel [13]. Mutations in *SCN1A* generally produce truncated proteins because they are either nonsense or trigger frameshifts or alter splice sites [14]. This pathology remains largely pharmaco-resistant. The mouse models of DS clearly recapitulate the human clinical phenotype [15]. Most of these Dravet phenotypes are preserved when the hypo-expression of $Na_v1.1$ is limited to parvalbumin-expressing inhibitory neurons by a conditional approach in mice [16]. It should be emphasized that patients or animals affected by DS can experience sudden unexpected death in epilepsy (SUDEP) [17], possibly linked to a direct or indirect role of $Na_v1.1$ in cardiomyocyte function [18], although this has not been formally established [19]. SUDEP is particularly problematic for the medical care as it may affect up to 20 % of the patients (and up to 50 % of Dravet mice) [20]. Of note, patients or animals that survive the onset and development of the pathology may do so because of compensatory mechanisms taking place through replacement of $Na_v1.1$ function by alternative isoforms. Other emerging disorders linked to *SCN1A* include autism spectrum disorder (ASD) [21], that appears to affect Dravet patients as well, and cognitive dysfunctions in Alzheimer disease (AD) models [22]. A particularly interesting observation is that human amyloid precursor protein transgenic mice and AD patients have decreased levels of $Na_v1.1$ channel in inhibitory parvalbumin cells. Restoring the expression levels of this channel type significantly alleviates epileptiform discharges and memory deficits [23].

Several therapeutic strategies have been envisioned to resolve $Na_v1.1$ haploinsufficiency in DS or in AD. One promising strategy consists of boosting $Na_v1.1$ expression levels by preventing the occurrence of non-productive alternative splicing and by favoring the generation of productive mRNA thanks to an antisense-mediated modulation of pre-mRNA splicing [23]. In the case of *SCN1A*, the concept behind this approach is to block by steric hindrance the inclusion within the mRNA of a naturally occurring alternatively spliced poison exon. The technique is called Targeted Augmentation of Nuclear Gene Output (TANGO) and seems to be efficient for treating Dravet syndrome at the preclinical level [24]. A more difficult approach consists in directing transcriptional activators towards the promoter of *SCN1A*. This approach was attempted using a CRISPR-activation technology and applied successfully for the conditional upregulation of *scn1a* in mice inhibitory neurons [25,26]. However, the use of viruses to achieve this result will undoubtedly represent a legal and safety issue for its applicability to human patients. Pharmacology is another, more straightforward, option. While stiripentol [27] and cannabidiol [28] have been approved by the U.S. Food and Drug Administration for managing epileptic seizures of DS patients, these drugs fall short of treating the larger panel of DS symptomologies.

The most common approach to DS is to develop pharmacological activators of $Na_v1.1$. Such a compound should ideally increase Na^+ influx without modification of the channel gating properties. However, this is problematic if maximal channel opening probability is already occurring for the remaining functional $Na_v1.1$ channels. The alternative option is to identify channel gating modifiers that would act by i) lowering activation threshold of $Na_v1.1$ channels, ii) shifting their midpoint of inactivation towards depolarized values or iii) slowing inactivation kinetics. Such an approach was successfully described by the use of a spider peptide, δ-theraphotoxin Hm1a (Hm1a), that slows $Na_v1.1$ channel inactivation [29,30] and allowed the identification of $Na_v1.1$ as an actor for mediating mechanical pain [30]. In the same studies, an analog of Hm1a was identified that possesses string sequence homology, δ-theraphotoxin Hm1b (Hm1b). Hm1a appears to bind to voltage-sensing domain IV of $Na_v1.1$, hindering both fast and slow inactivation [31]. Hm1a successfully restored the normal firing activity of GABAergic interneurons in a DS mouse model and alleviated epileptic seizures. It seems also potent in rescuing DS mice from seizures and SUDEP upon intracerebroventricular infusion [32]. There are, however, several issues with Hm1a use for treating DS that need to be better apprehended. First, the peptide is not fully selective for $Na_v1.1$ since overlap of activity was reported for $Na_v1.2$ and $Na_v1.6$ [30,33], thereby reducing the therapeutic safety window. Second, preservation of channel selectivity of the peptide towards mice and human Na_v isoforms is not well studied. There are substantial sequence differences in the extracellular loops between human and mouse Na_v channels for a given isoform and for Hm1a to become an interesting lead compound for human DS based on mouse DS data, the respective isoform selectivity of the peptide should be preserved across species. Third, Hm1a is particularly difficult to synthesize owing to an amino acid sequence that reduces the yield of the rather specific disulfide bridge pairing of the peptide generally observed in Inhibitor Cystine Knot (ICK)-folded toxins (C_1–C_4, C_2–C_5 and C_3–C_6 pairing architecture). Fourth, Hm1a is unstable in cerebrospinal fluid [29]. A low yield of production, combined with a low therapeutic window, and a lack of clarity on the exact selectivity of Hm1a for human Na_v isoforms compared to mouse orthologs, handicap the therapeutic potential of this peptide. It is therefore essential to search for novel $Na_v1.1$-selective compounds that could eventually match Hm1a's potential for DS treatment, as well as to understand the molecular basis of natural peptides for selective human $Na_v1.1$ channel activity stimulation. Moreover, it is important to define the amino acid sequence determinants that allow easy refolding of such an activator, posing the conditions for a facilitated production yield. A similar endeavor had been undertaken for a recombinant extended form of Hm1b [29].

Herein we describe the identification of a previously partially characterized spider peptide, JzTx-34, mediated by a functional screen on $hNa_v1.1$ channels. Although JzTx-34 was previously reported as an inhibitor of $Na_v1.7$, we report more potent activity as an activator of $hNa_v1.1$. We performed a highly enriched selectivity profiling of this toxin combined with a full structural analysis that comprises structure determination, alanine scan and structural impact of this scan. As this peptide possesses a limited sequence homology with Hm1a, it also helps to understand the structural determinants involved in folding and selectivity of $Na_v1.1$ active peptides.

2. Methods

2.1. Chemical syntheses of JzTx-34 and its analogs

Linear JzTx-34 and analogs were assembled stepwise using fmoc solid-phase peptide synthesis (SPPS) on a Symphony synthesizer (Protein Technologies Inc.), at a 0.1 mmol scale on 2-chlorotrityl chloride resin (substitution approx. 1.6 mmol/g). Fmoc-protecting group was removed using 20 % piperidine in dimethylformamide (DMF) and free amine was coupled using tenfold excess of Fmoc amino acids and HCTU/DIEA activation in NMP/DMF (3 × 15 min). The linear peptides were

deprotected and cleaved from the resin with TFA/H_2O/1,3-dimethoxybenzene/TIS 92.5/2.5/2.5/2.5 (vol.), then precipitated out in cold diethyl ether. The resulting white solids were washed two times with diethyl ether, re-suspended in H_2O/acetonitrile and freeze dried to afford crude linear peptide. The crude peptides were folded by air oxidation at 25 mM in a 200 mM ammonium acetate buffer at pH 7.8, containing 5 mM GSH and 0.5 mM GSSG. After 24–72 h (dependent on analog sequence) at 4 °C the pH of the reaction mixtures was adjusted to 3.0 and purified by preparative HPLC as follows: a first purification by reverse-phase HPLC on a C18 Phenomenex Luna stationary phase on an Agilent Technologies preparative HPLC system (eluent system H_2O/MeCN + 0.1 % TFA), then, if necessary, a second purification by SCX on an Agilent SCX NP5 column on a semi-preparative HPLC system (eluent system 20 mM phosphate buffer pH 6.0, 1 M NaCl, 20 % MeOH, 20 % MeCN). A final desalting step afforded pure synthetic JzTx-34 (over 6 % overall yield) or its analogs (between 0.1 % and 8.6 % yield without optimization). Homogeneity of the synthetic folded native peptide sequence with the natural JzTx-34 peptide was assessed by coelution on an analytical scale.

2.2. Cell cultures

HEK-293 cells stably expressing the $hNa_v1.1$ (XM_011511604), $hNa_v1.2$ (XM_017004655), $hNa_v1.3$, $hNa_v1.4$, $hNa_v1.5$ or $hNa_v1.6$ channel subtype (XM_011538651) or hERG channels (NM_000238) were cultured in Dulbecco's Modified Eagle's Medium (DMEM) supplemented with 10 % fetal calf serum, 1 mM pyruvic acid, 4.5 g/L glucose, 2 mM glutamine, 800 μg/mL G418, 10 U/mL penicillin and 10 μg/mL streptomycin (Gibco, Grand Island, NY). CHO cells stably expressing the $hNa_v1.7$ channel subtype (XM_011511618) were cultured in Dulbecco's Modified Eagle's Medium F-12 (DMEM/ F12) supplemented with 10 % fetal bovine serum, 2 mM glutamine, 200 μg/mL hygromycin B, 10 U/mL penicillin and 10 μg/mL streptomycin (Gibco, Grand Island, NY). All cell lines were incubated at 37 °C in a 5 % CO_2 atmosphere and used between passaging number 20 and 40.

2.3. Sodium influx assays

The sodium influx assays employ the cell permeable, sodium-sensitive Asante Natrium Green-2 (ANG2) dye to quantify sodium ion influx through sodium channels, which are maintained in an open-state by use of the sodium channel modulator veratridine. These high-throughput sodium influx assays allow for rapid profiling and characterization of sodium channel modulators. Briefly, TREX HEK-293 cells were stably transfected with an inducible expression vector containing the full-length cDNA coding for the desired human sodium channel α-subunit, full-length cDNA coding for inward rectifying potassium channel, Kir1.1, and with an expression vector containing full-length cDNA coding for the β1-subunit. Sodium channel expressing cell lines were induced with tetracycline (1 μg/mL) and plated on 384-well poly-D-lysine (PDL)-coated plates at a density of 25 K cells/well in culture media (DMEM, containing 10 % FBS and 1 % L-glutamine). After overnight incubation (37 °C, 5 % CO_2), culture media was removed and cells were loaded with 5 μM ANG2 dye for 1 hr in buffer 1 (155 mM N-methyl-D-glucamine, 5 mM KCl, 2 mM $CaCl_2$, 1 mM $MgCl_2$, 10 mM 4-(2-hydroxyethyl)-1-piperazineethanesulfonic acid (HEPES), 10 mM glucose, adjusted with Tris to pH 7.4). Excess dye was removed and cells were incubated with and without test compound for 1 hr in buffer 1 containing 100 μM veratridine. A Hamamatsu FDSS μCell was used to perform a 1:1 addition of Na/K challenge buffer (145 mM NaCl, 20 mM HEPES, 1 mM $CaCl_2$, 15 mM KCl, 1 mM $MgCl_2$, 10 mM glucose, adjusted with Tris to pH 7.4) and simultaneously read plates at excitation wavelength of 530 nm and emission wavelength of 558 nm. Non-sodium channel mediated sodium influx was determined in the presence of 1 μM tetrodotoxin (TTX). This background signal was subtracted from the total sodium influx signal in the absence of venom fraction, and all data in the presence of venom fraction, purified or synthetic peptide was normalized to this control. Percent inhibition or activation of sodium ion influx was calculated for each test sample. The sodium influx assays were confirmed by the use of a Sophion cube automated patch-clamp, homed at Xenon Pharmaceuticals.

2.4. Automated high-throughput patch-clamp experiments and pharmacology

The JzTx-34 analogs were investigated on HEK-293 cells expressing $hNa_v1.1$, $hNa_v1.2$, $hNa_v1.3$, $hNa_v1.4$, $hNa_v1.5$ or $hNa_v1.6$ channel and CHO cells expressing $hNa_v1.7$ channel using the automated patch-clamp system from Nanion (SyncroPatch 384PE, München, Germany). For electrophysiological recordings, cells were detached with trypsin, and floating single cells were diluted (~ 300,000 cells/mL) in an extracellular solution containing (in mM): 140 NaCl, 4 KCl, 2 $CaCl_2$, 1 $MgCl_2$, 5 glucose and 10 HEPES (pH 7.4, osmolarity 312 mOsm), that was used throughout the experiments. Chips with single-hole and medium-resistance (~ 4.5 MΩ) were used for all cell lines. Voltage pulses and whole-cell recordings were achieved using the PatchControl384 v1.5.2 software (Nanion) and the Biomek v1.0 interface (Beckman Coulter). Prior to recordings, dissociated cells were shaken at 200 RPM in a cell hotel reservoir at 10 °C. After cell catching, sealing and whole-cell formation, protocol application, compound administration and data acquisition were all performed sequentially and automatically. The intracellular solution contained (in mM): 110 CsF, 10 CsCl, 10 NaCl, 10 EGTA and 10 HEPES (pH 7.2, osmolarity 260 mOsm) and the extracellular solution, in which cells were incubated, was used. Whole-cell experiments were done at − 100 mV holding potential and at room temperature (18–22 °C), while currents triggered at either + 10 mV test potential were sampled at 20 kHz. Stimulation frequency was set at 0.2 Hz. Each JzTx-34 analog was prepared at various concentrations in the extracellular solution, itself supplemented with 0.3 % of bovine serum albumin (BSA), also added in the control solution. The peptides were distributed in 384-well microplates according to the number of compounds to be tested (generally three per plate), the concentration range grossly defined from the IC_{50} of wild-type JzTx-34, and the number of cells desired for each experimental condition. Compound solutions were diluted 3 times in the patch-clamp recording well by adding 30 μL external solution, to reach the final reported concentration and the test volume of 90 μL. For establishing concentration-response curves, the compounds were tested at a test potential of + 10 mV for 50-ms with a pulse every 5 s. Percentages of current inhibition were measured at steady-state of effect at the end of a 15-min application time.

2.5. NMR acquisition

A 0.1 mM solution of JzTx-34 in H_2O/D_2O (90/10) at pH 4.5 was prepared in a 3-mm tube. Each mutant was prepared the same way, namely W^5A, L^6A, $H^{18}A$, $L^{19}A$, $E^{20}A$, $R^{22}A$, $W^{25}A$, $V^{30}A$, $W^{31}A$ and $W^{33}A$. All NMR spectra were acquired at 298 K on a BRUKER 700 MHz spectrometer equipped with a 5 mm TCI cryoprobe, namely COSY, 80-ms TOCSY, 160-ms NOESY, $^1H/^{15}N$ SoFast-HMQC, and $^1H/^{13}C$ HSQC, and were processed with TopSpin3.2.

2.6. Chemical shift assignments and structure calculations

Classical procedures were followed to assign chemical shifts, with CcpNmr2.1 software [34]. NMR constraints were deduced from the volume integration of NOE correlations and introduced into the iterative calculation process of the Aria2.3 software [35]. In each run, 500 structures were calculated per iteration, and 250 structures were kept for the final iteration in water. 0nly NOE-derived constraints were introduced in the calculation, all combinations of disulfide bridges pairing being allowed with the ambiguous intersulfur constraints option of ARIA. Quality of the final structures were evaluated using

Procheck3.5 [36] software, and ten representative structures were selected according to their agreement with experimental and energetic data (residual NOE violation, Ramachandran plot, energy values …).

2.7. Statistical analyses

Values are represented as mean ± SEM. Significance was tested by performing paired non parametric t-test *in vivo* experiments. A p-value lower than 0.05 was considered significant.

3. Results

3.1. Venom screening and discovery of a previously unnoticed hNa$_v$1.1 activator

In a global initiative to identify several novel peptides active on Na$_v$

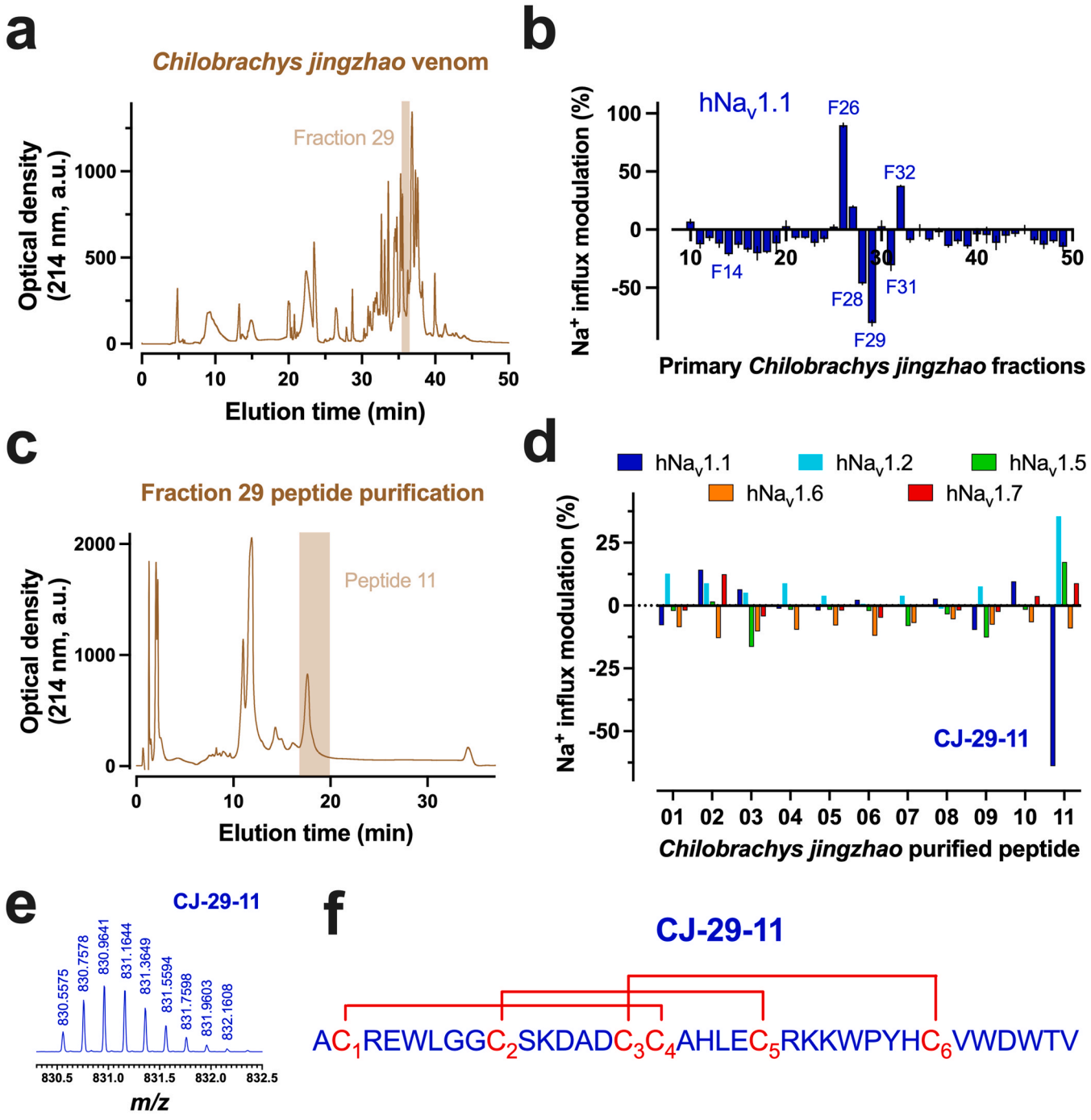

Fig. 1. Discovery and identification of CJ-29-11 as an activator of hNa$_v$1.1 channel. (**a**) Semi-preparative RP-HPLC fractionation of *Chilobrachys jingzhao* venom showing the distribution of the material as a function of elution time. The position of fraction 29 elution is shown by a brown box. (**b**) Effects of fractions (F) 10–49 on sodium influx mediated by hNa$_v$1.1 activated by veratridine. As shown, F14, F28, F29 and F31 are activator fractions (downward shifts by convention), whereas F26 and F32 are inhibitor fractions (upward shifts by convention). Modulation beyond 20 % was considered significant. (**c**) Cation exchange purification of F29, the most active fraction for activation of hNa$_v$1.1. The elution time of peptide 11 is shown by the brown box. (**d**) Effect of each purified peptide from F29 on hNa$_v$1.1-mediated Na$^+$ influx. As shown, only peptide 11 has a maximal stimulation effect. This natural peptide is termed CJ-29-11. (**e**) ESI-MS spectrum of [CJ-29-11 + 5H]$^{5+}$ showing an m/z = 830.5575, yielding an experimental molecular weight of 4147.82 Da. (**f**) Primary structure of CJ-29-11. Disulfide bridges are shown in red.

channels, we screened 90 venoms from different species (1 marine cone, 1 fish, 1 bee, 2 lizards, 3 wasps, 4 centipedes, 5 batrachians, 15 scorpions, 22 spiders and 41 snakes) on five human Na_v channel targets ($Na_v1.1$, $Na_v1.2$, $Na_v1.5$, $Na_v1.6$ and $Na_v1.7$) using a sodium influx assay. Spider venoms provided the greatest hit rates in this study indicating that they represent a better source for the identification of novel natural peptides active on Na_v channels. Furthermore, spider venoms regularly provided channel activators, in addition to inhibitors, which, in the framework of our search for $hNa_v1.1$ activators, represents an additional incentive for using these venom sources. The screening process followed a two-step rationality: an initial screening based on channel modulation by primary RP-HPLC fractions of the venom, in which several natural compounds were present (from 3 to 11 depending on fraction number and venom type), and a second screening step using purified individual compounds from positive primary fractions. Care was taken to preserve the same peptide concentration in both screening steps (variable depending on peptide nature). Only one out of the 22 spider venoms tested lacked a fraction capable to modulate $hNa_v1.1$ activity indicating a success rate of 95 % for venoms from the arachnid class. On the 21 positive venoms, 6 venoms yielded only $hNa_v1.1$-activating fractions, 4 venoms only $hNa_v1.1$-inhibiting fractions, and the remaining 11 venoms yielded both activating- and inhibiting-fractions. These basic considerations indicate the high potential for discovering numerous peptides active on Na_v channels out of spider venoms. The second most important sources for Na_v channel modulators were scorpion venoms as 13/17 of them provided primary fractions active on Na_v channels. For this present report, we focused our analysis on identifying a $hNa_v1.1$-activating peptide from the venom of *Chilobrachys jingzhao* (CJ) Chinese tarantula spider. This spider venom was chosen because i) it has been extensively studied before [37–47], which facilitates the identification of positive hits, and ii) it provided many primary fraction hits active on various Na_v channels, both activators and inhibitors, enhancing the chances for discovering interesting compounds. The venom was first separated into 64 fractions (F) by semi-preparative RP-HPLC. Most of the material was segregated within 8–49 min elution times and we decided therefore to screen from F1 up to F49 that comprised all of this material (Fig. 1a). Six primary fractions (F) were found active on $hNa_v1.1$ (F14, F28, F29 and F31 increased sodium influx, while F26 and F32 inhibited it) beyond the threshold level of 20 % modulation of Na^+ influx (Fig. 1b). Six fractions modulated also $hNa_v1.2$ (F16 and F31: activating; F25, F26, F27 and F32: inhibiting) (Fig. S1a). Concerning $hNa_v1.5$, only two activating fractions were identified (F13 and F31) (Fig. S1b), while for $hNa_v1.6$, three fractions modulated this channel type (F31 and F33: activating; F26: inhibiting) (Fig. S1c). Finally, four contiguous fractions inhibited $hNa_v1.7$ (F25–F28) (Fig. S1d). As such, both fractions F28 and F29 were relatively specific for activating $hNa_v1.1$ and were thus studied further, along with F30 for comparison purposes as it lacked activity on all Na_v isoforms tested. These three fractions were studied again on all five Na_v channel isoforms using different dilution factors to modulate compound concentrations in these fractions. As a reminder, primary venom fractions are simplified, but still complex, mixtures that contain a number of compounds differing in concentrations. Using different dilution factors of these primary fractions may result in some compounds keeping activity, while others losing activity because they are present below their effective concentration. A change in Na_v channel subtype selectivity was indeed observed upon using different dilution factors for each of these primary fractions, F28, F29 and F30 (Fig. S2). Major $hNa_v1.1$-activating potency was observed for F28 and F29 at low dilution factors (20–150 ×), but this activity was lost at higher dilution factors (300 × or above). Interestingly, F30 revealed some $hNa_v1.1$-blocking activity at higher dilution factors, suggesting that, at low dilution factors, this fraction may contain both activating and inhibiting compounds that provide a global negative readout. F30 is thus a false negative and may contain compounds of interest, coherent with the general observation that the more you purify venoms, the more you increase the hit rate in a screening assay. We next focused on fraction F29 to purify a $hNa_v1.1$-activating compound from this venom. Peptide components of F29 were purified by cation exchange (Fig. 1c). Eleven peptides were obtained according to this procedure and tested for their ability to regulate $hNa_v1.1$-mediated Na^+ influx (Fig. 1d). As shown, only peptide 11 (identified herein by the code number CJ-29-11) had the capability to stimulate $hNa_v1.1$ Na^+ influx, while it also showed some blocking potential on the $hNa_v1.2$ channel isoform. CJ-29-11 was submitted to an LC-ESI QTOF MS analysis and provided an $[CJ\text{-}29\text{-}11 + 5H]^{5+}$ m/z value of 830.5575 (Fig. 1e). This corresponds to an experimental mass of 4147.8 Da for this $Na_v1.1$-activating peptide.

3.2. Sequence determination of CJ-29-11 and search for analogs

The primary sequence of natural CJ-29-11 was determined by a combination of analytical techniques including a bottom-up approach with high resolution mass spectrometry (Fig. 1f). According to the data, CJ-29-11 does not contain any post-translational modification (except the formation of disulfide bridges). It is a 35 amino acid peptide with six cysteine residues involved in 3 disulfide bridges. A blast search provided important information on related peptides. Unsurprisingly for an extensively studied spider specie, the sequence of CJ-29-11 had been determined earlier and this peptide had been termed Jingzhaotoxin-34 (JzTx-34) [37,48]. JzTx-34 was reported to inhibit TTX-sensitive sodium channels in rat DRG neurons and the effect on $hNa_v1.1$ was unknown. The structure of JzTx-34 conforms to an inhibitor-cysteine knot (ICK) type of fold that is regularly identified in spider venoms. ICK peptides are generally difficult to chemically synthesize, particularly if the third and fourth cysteine residue within the peptide chain are contiguous as it is the case here and for Hm1a. The blast search also allowed the identification of closely related peptides, namely μ-TrTx-Phlo1a and μ-TrTx-Phlo1b, which possess the same length as JzTx-34 and differ by only 3 residues at positions 5, 13 and 35, and by C-terminal amidation (Fig. 2). JzTx-34 sequence was also aligned with that of Hm1a, another reputed $hNa_v1.1$ activator [29,31,32], and shown to be significantly different (Fig. S3a).

3.3. Chemical synthesis of JzTx-34

Chemical synthesis of JzTx-34 was performed by SPPS using a scale of 0.1 mmol of linear peptide. The different steps of chemical synthesis are described (Fig. 3). The linear peptide eluted at 21.0 min (Fig. 3a). Folding and oxidation was performed in classical conditions, using a redox couple GSH/GSSG and, contrary to Hm1a, occurred spontaneously, indicating that the sequence was intrinsically favorable to folding. Upon folding two peaks appear with a ratio of 30/70 (30 % for the first eluting peak and 70 % for the second eluting peak, which is the one that holds activity). The elution time of the second eluting peak was 22.7 min (Fig. 3b). Following purification (Fig. 3c), the yield of synthesis could be estimated at 6.3 % at a purity exceeding 99.5 %. A total of 26.05 mg was obtained (quantified by UV dosing at 280 nm with a theoretical epsilon 23865), corresponding to 6.3 μmol. LC-ESI QTOF mass spectrometry confirmed that the synthetic JzTx-34 (m/z value for $[JzTx\text{-}34 + 5H]^{5+}$ of 830.5644) had the same mass as the purified CJ-29-11 peptide (Fig. 3c). Finally, we performed coelution experiments that further confirmed the perfect identity between synthetic JzTx-34 and the natural purified CJ-29-11 peptide (Fig. 3d**).** It can be concluded that JzTx-34, a $hNa_v1.1$ channel activator, is easier to synthesize than Hm1a, which requires directed disulfide bridge formation and is obtained at much lower yield.

3.4. Pharmacological characterization of JzTx-34

Identifying JzTx-34 as a $hNa_v1.1$ channel activator was surprising because a first report indicated a lack of effect of this peptide on this channel subtype [48]. However, in this report, the authors used rat

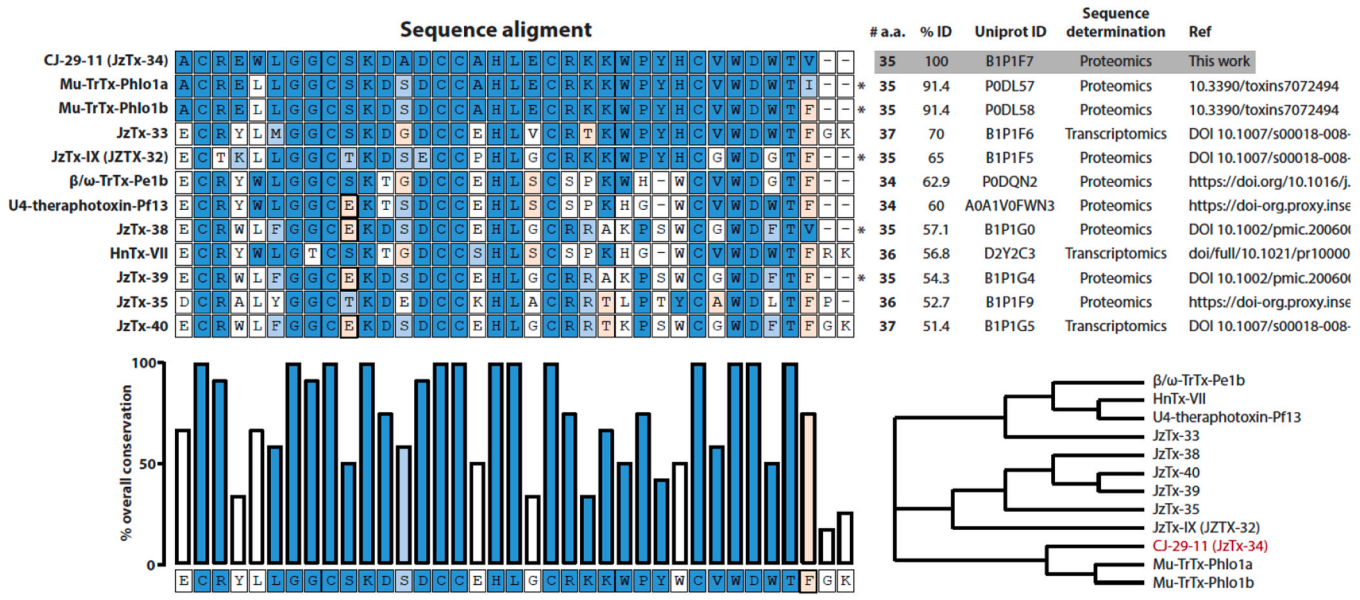

Fig. 2. Sequence alignment of JzTx-34 with closely related natural peptides. C-terminal amidation is represented by *. Sequences that have been determined by transcriptomic analyses do not inform of potential post-translational modifications. Conservation of residues is shown at the bottom left (dark blue: strictly conserved residues; light blue: conserved substitutions; salmon: semi-conserved residues; white: absence of conservation), while a phylogenic tree illustrates the two most closely related peptides to JzTx-34 (mu-TrTx-Phlo1a and mu-TrTx-Phlo1b). Hm1a, a potent activator of $hNa_v1.1$, is too divergent and does not appear in the list.

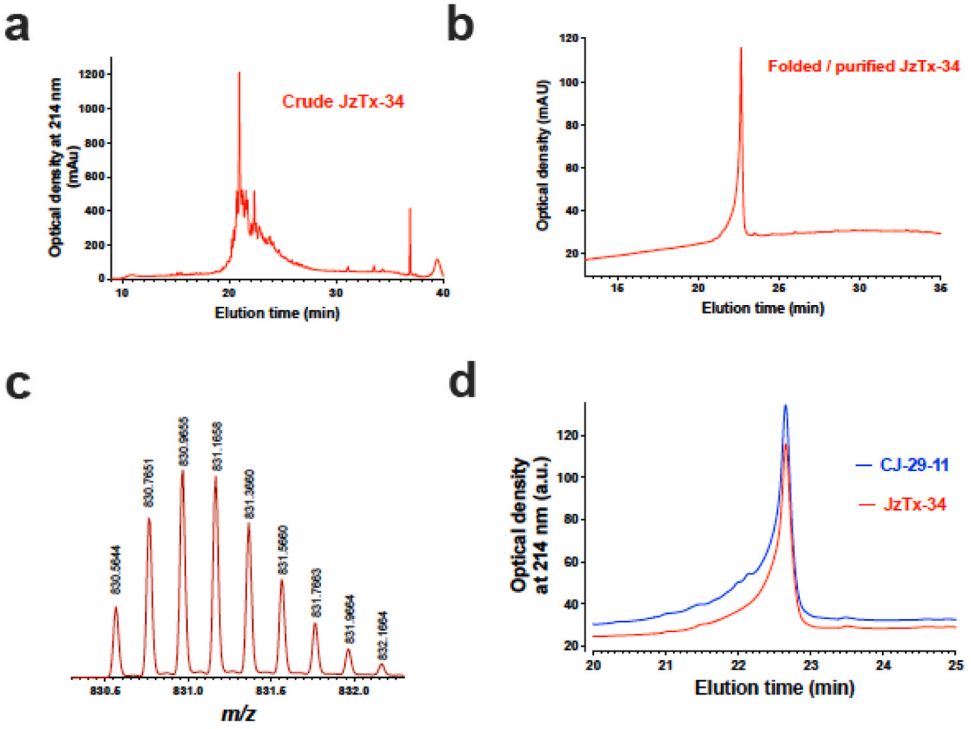

Fig. 3. (**a**,**b**) Analytical RP-HPLC chromatogram illustrating the elution profiles of crude unfolded, folded/oxidized and purified JzTx-34, respectively. (**c**) ESI-MS spectrum of $[JzTx\text{-}34 + 5H]^{5+}$ showing an $m/z = 830.5644$, yielding an experimental molecular weight of 4147.82 Da. (**d**) Elution experiments showing the LC-UV traces at 214 nm of natural CJ-29-11 and synthetic JzTx-34 peptides, both eluting at 22.6 min.

$Na_v1.1$ instead of the human orthologue and since there are several differences in the amino acid sequences of the external loops within the voltage sensors between rodent and human $Na_v1.1$, it was possible that JzTx-34 does not bind to rat $Na_v1.1$. To test this issue, rat $Na_v1.1$ was expressed in *Xenopus laevis* oocytes and several concentrations of synthetic JzTx-34 were tested. As shown, no effect was observed at 1 μM JzTx-34, while it took 5 μM to get a minimal effect of inactivation kinetic slowing (Fig. S4). These results explain the observed apparent discrepancy with the earlier study on JzTx-34 and provide interesting lead data for investigating JzTx-34 binding site on $hNa_v1.1$. We next pursued our investigation by studying the effects of synthetic JzTx-34 to better understand its mode of action, potency and selectivity. Using the same Na^+ influx assay (Fig. 1) as the one that allowed the identification of CJ-29-11 as a $hNa_v1.1$ activator, we confirmed that increasing

concentrations of JzTx-34 lead to increased Na^+ influx with an EC_{50} of 351 nM and a maximal amplitude of stimulation of 140.4 % (Fig. 4a). In addition, coherent with the Fig. 1 data using the native peptide, JzTx-34 inhibits Na^+ influx through $hNa_v1.2$ with an IC_{50} of 318 nM and a maximal inhibition of 96.6 %. Lower inhibitions were observed for $hNa_v1.6$ and $hNa_v1.7$ with IC_{50} values of 4.4 μM and 6.6 μM, respectively. These inhibitions were largely incomplete. To get a more precise picture on the mode of action of JzTx-34 on Na_v channels, we turned towards automated patch-clamp recordings to assess the impact of the peptide on both $hNa_v1.1$ current kinetics and peak amplitudes. As shown, increasing concentrations of JzTx-34 had little effects on Na^+ peak currents of $hNa_v1.1$ but inhibited fast inactivation with progressively greater efficacies (Fig. 4b). Both effects were quantified. Normalized peak current amplitudes did not vary significantly up to 1 μM of JzTx-34 (Fig. 4c). In contrast, if the integrals of $hNa_v1.1$-mediated currents were measured over the pulse duration, then a very significant 9.8-fold stimulation of Na^+ entry is detected with an EC_{50} of 42.9 nM (8.2-fold better EC_{50} value than with the Na^+ influx assay (351 nM)). The extent of stimulation is also higher than with the Na^+ influx assay using a Na^+-sensitive dye (see Fig. 4a). These differences might occur because, in the flux assay, veratridine, used in this type of assay, modifies activation and inactivation, thereby impacting the effect of JzTx-34 and possibly also its affinity for the channel. To identify the binding domain with which JzTx-34 is interacting to produce its functional effects on $hNa_v1.1$, we tested the peptide on chimeras between $K_v2.1$ and $hNa_v1.1$ in which the S3–S4 loop of the voltage sensor domain (VSD) of $K_v2.1$ was replaced by one of the four different VSDs of $hNa_v1.1$ (I to IV) [49,50]. As shown, application of JzTx-34 fully inhibits the chimera in which $hNa_v1.1$ VSDIV was integrated into $K_v2.1$ (Fig. 4d), which is compatible with the notion that toxins that bind VSDIV in Na_v channels inhibit inactivation [31]. Interestingly, a mild effect is also observed on chimeras that integrated VSDII, a VSD associated with channel gating inhibition. We assume that it may be linked to a second binding site of lower affinity that may be involved in channel inhibition, namely those observed on other Na_v isoforms (Fig. 4a & Fig. 5).

3.5. Selectivity of JzTx-34

Since the effect of JzTx-34 on $hNa_v1.1$ had not been noticed earlier [37,48], because of the use of the rat Na_v channel sequence instead of the human one, we further pursued the study of the selectivity of JzTx-34 for human ion channels. Two aspects were investigated for each of the Na_v channel isoforms: i) peak current reduction and ii) slowing of channel inactivation kinetics that were quantified by the integrals of the current (Area Under the Curve, AUC). As shown, all the tested channels were sensitive to JzTx-34 albeit at higher concentrations than $hNa_v1.1$ (Fig. 5). JzTx-34 blocks $hNa_v1.2$, $hNa_v1.4$, $hNa_v1.5$, $hNa_v1.7$ and hERG channel peak currents with IC_{50} values of 998 nM, > 3 μM, 434 nM, 379 nM and 852 nM, respectively (Fig. 5a, c, d, f, h). The effect on $hNa_v1.7$ is consistent with the earlier report where they indicate inhibition with an IC_{50} of 610 nM instead of 379 nM here [48]. However, not all the other effects on the other channels had been detected, again indicating that species differences in Na_v channel sequences may be instrumental. Our data using human clones indicate that the peptide possesses a selectivity ratio comprised between 8.8- and > 71-fold for $hNa_v1.1$, making JzTx-34 selective for $hNa_v1.1$, especially if low effective concentrations are used to activate $hNa_v1.1$. For instance, none of the other channel types were affected by 10 or 33 nM JzTx-34,

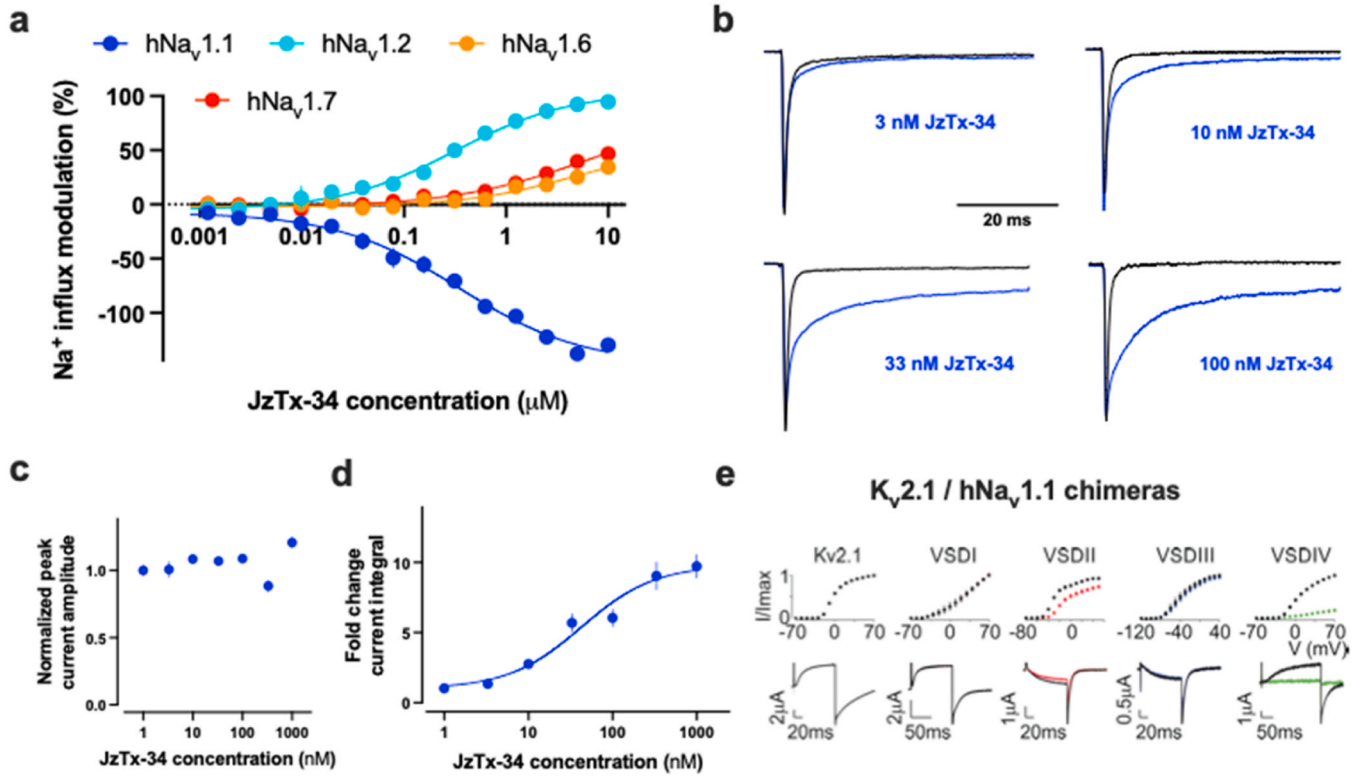

Fig. 4. (**a**) Sodium influx experiments evaluating the concentration-dependent effects of synthetic JzTx-34 on four different hNa_v isoforms ($hNa_v1.1$, $hNa_v1.2$, $hNa_v1.6$ and $hNa_v1.7$). Positive modulation corresponds to influx inhibition, while negative modulation represents stimulation. Fits of the data yield IC_{50} values of 318 nM ($hNa_v1.2$, Hill value 0.77), 4.4 μM ($hNa_v1.6$, Hill value 0.83) and 6.6 μM ($hNa_v1.7$, Hill value 0.65) and EC_{50} value of 351 nM ($hNa_v1.1$, Hill value − 0.72). (**b**) Representative whole-cell recordings of $hNa_v1.1$ current before and after increasing concentrations of JzTx-34 showing the increasing effect on inactivation kinetics. (**c**) Average effect of increasing JzTx-34 concentrations on peak current amplitude (n = 23). (**d**) Average effect of increasing JzTx-34 concentrations on current integrals. Data fit yield an EC_{50} value of 42.9 nM and a maximal current stimulation of 9.8-fold (n = 23). (**e**) Average effect of 100 nM JzTx-34 on $K_v2.1$/$hNa_v1.1$ chimeras in which the VSD of $K_v2.1$ was replaced by one of the four VSD of $hNa_v1.1$. Maximal inhibition is seen when the VSDIV of $hNa_v1.1$ is used.

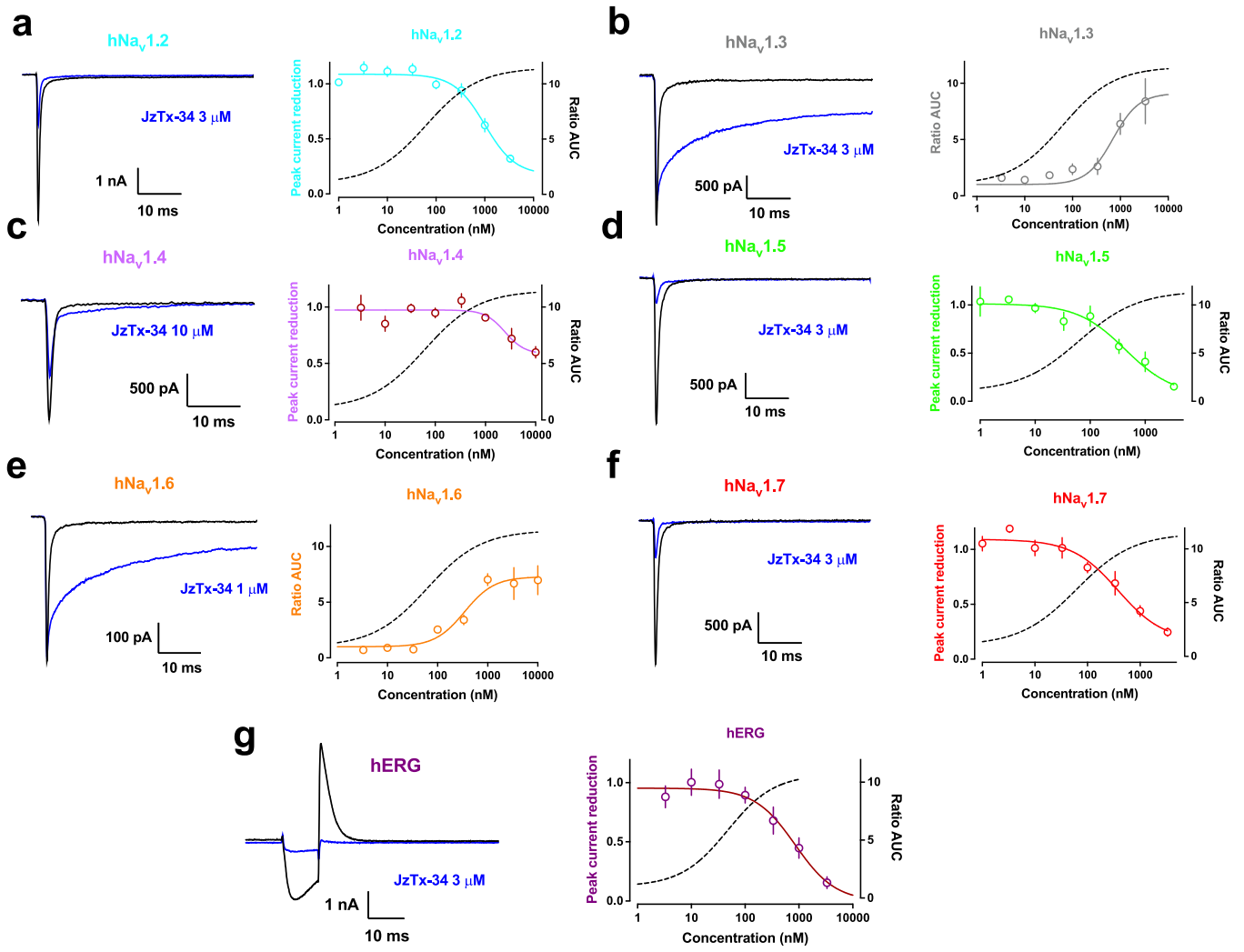

Fig. 5. Channel selectivity of JzTx-34. (**a**) Left: representative $hNa_v1.2$ current before and after block by 3 μM JzTx-34. Right: average dose-response effect of JzTx-34 on $hNa_v1.2$ channel (n = 11). In contrast to the effect of JzTx-34 on $hNa_v1.1$ (dashed line) by blocking inactivation as measured by the area under the curve (AUC) ratio (under JzTx-34 over control), JzTx-34 blocks current amplitude of $hNa_v1.2$ with an IC_{50} of 998 nM. (**b**) Left: representative $hNa_v1.3$ current stimulation by 3 μM JzTx-34. Right: average dose-response effect of JzTx-34 on $hNa_v1.3$ illustrating the increase in AUC with an EC_{50} of 698 nM and a maximal stimulation of 9.1-fold (n = 6). (**c**) Left: representative effect of 10 μM JzTx-34 on $hNa_v1.4$ current illustrating a mixed response characterized by peak amplitude reduction and mild slowing of inactivation. Right: average dose-response curve of JzTx-34 on peak current amplitude of $hNa_v1.4$ (n = 9). IC_{50} value exceeds 3 μM and could not be determined. (**d**) left: representative effect of 3 μM JzTx-34 on $hNa_v1.5$ illustrating peak current reduction. Right: average dose-response curve for JzTx-34 inhibition of peak $hNa_v1.5$ currents with an IC_{50} of 434 nM (n = 7). (**e**) Left: representative effect of 1 μM JzTx-34 on $hNa_v1.6$ illustrating slowing of inactivation with concomitant increase in AUC. Right: average dose-response curve of JzTx-34 on AUC of $hNa_v1.6$ currents with an EC_{50} value of 346 nM and a maximal stimulation of 7.3-fold (n = 8). (**f**) Left: representative peak current inhibition of $hNa_v1.7$ by 3 μM JzTx-34. Right: dose-response curve of JzTx-34-mediated peak current inhibition of $hNa_v1.7$ with an IC_{50} value of 379 nM (n = 7). (**g**) Left: Representative current trace of hERG currents and its peak inhibition by 3 μM JzTx-34. Right: average dose-response curve of hERG peak current inhibition by JzTx-34 with an IC_{50} value of 852 nM (n = 9).

concentrations that produce significant $hNa_v1.1$ activation (Fig. 4b,d). The absence of effect of these JzTx-34 concentrations on $hNa_v1.5$ and hERG channels are also first encouraging signs that this peptide should lack cardiac toxic effects. Further proof of this lack of toxicity comes from ECG recordings in mice, in which 500 μg/kg body weight were injected intravenously (Fig. S5). No modification of the ECG traces could be monitored over 10 min recordings post-injection of JzTx-34 apart from a minor prolongation of the QT interval but that is insufficient to produce rhythm disorder. Cardiac exposure to the peptide would however be a minor issue if it had to be injected directly into the central nervous system. For three of the other ion channels tested ($hNa_v1.3$, $hNa_v1.4$ and $hNa_v1.6$), JzTx-34 produced a slowing of inactivation. In the case of $hNa_v1.4$, this slowing of inactivation did not translate itself into an AUC increase since a concomitant peak current inhibition occurred at overlapping concentrations (Fig. 5c). As a result, the concentration-response effect of JzTx-34 on peak current inhibition was incomplete because of the competing converse effect on AUC as shown by the representative trace at 10 μM JzTx-34. We interpret these data by the likelihood that JzTx-34 possesses two binding sites on $hNa_v1.4$, one leading to current inhibition and another to inactivation kinetics inhibition. As shown in Fig. 4e, JzTx-34 binds to voltage-sensor domains II and IV, with a dominant effect on VSDIV. Spider toxins that bind to VSDII, such as ProTx2, inhibit activation, which can account for the reduction in peak inward current. For those isoforms that bind JzTx-34 less potently in VSDIV, the effect on binding to VSDII is likely more significant. In the case of $hNa_v1.3$ and $hNa_v1.6$, JzTx-34 produced significant AUC increases, but this occurred at higher concentrations (EC_{50} values of 698 nM and 346 nM, respectively, *versus* 42.9 nM for $hNa_v1.1$) and with lower amplitudes at maximal concentrations (9.1- and 7.3-fold, respectively, *versus* 9.8-fold for $hNa_v1.1$) (Fig. 5b, e). Here again, the

data obtained on these isoforms differ from the previous report [48], namely on $Na_v1.3$ since JzTx-34 inhibits rat $Na_v1.3$ with an IC_{50} of 7950 nM, whereas in our study it stimulates human $Na_v1.3$ with an EC_{50} of 698 nM. Globally, these electrophysiological results are coherent with our Na^+ influx assays (Fig. 4a), except maybe for $hNa_v1.6$ where inhibition was seen in influx assays and stimulation is observed here. The patch-clamp assay shows itself more sensitive than the Na^+ influx assay. It differs also fundamentally with the Na^+ influx assay by the fact that veratridine is not used to pre-activate the Na_v channels with all the inherent risks associated with drug interferences or state-dependent effects of JzTx-34.

To get a first hint on the structural determinants involved in the modification of inactivation of $hNa_v1.1$ by JzTx-34, we compared the activity of this peptide with that of Hm1a (Fig. S3a) that also slows inactivation of $hNa_v1.1$. Hm1a has the same length as JzTx-34 (35 amino acids), the same position of cysteine residues and lacks C-terminal amidation. There are however notable differences such as the missing H^{28} residue and limited sequence identity with JzTx-34 (54 %). Beside the 6 cysteine residues, there are 13 additional residues strictly conserved between JzTx-34 and Hm1a (Fig. S3a). The activities of Hm1a on $hNa_v1.1$ and $hNa_v1.2$ were compared to those of JzTx-34 in identical conditions. Low but significant slowing of $hNa_v1.1$ current could be observed at concentrations as low as 1 nM for Hm1a, while maximal effect was observed at 100 nM (Fig. S3b). The maximal slowing induced by Hm1a was comparable to that produced by JzTx-34 (close to 10-fold increase in AUC value), but the EC_{50} occurred at 3.5 nM for Hm1a compared to 42.9 nM for JzTx-34. A striking difference between JzTx-34 and Hm1a is the fact that JzTx-34 inhibits the peak current amplitude of $hNa_v1.2$, while leaving the inactivation process intact. The exact opposite is observed for Hm1a that inhibits $hNa_v1.2$ inactivation kinetics with EC_{50} of 124.1 nM based upon the AUC with a maximal stimulation of 9.3-fold (Fig. S3c). While both peptides are more selective for $hNa_v1.1$, JzTx-34 simultaneously activates $hNa_v1.1$ and inhibits $hNa_v1.2$ at higher concentrations, which is not the case for Hm1a, thereby preventing possible confusing interpretations for these two closely related channel types expressed in neuronal tissues. To get a better grip on the structural determinants of JzTx-34 important for $hNa_v1.1$ modulation, we performed an extensive investigation of the structure-activity relationship (SAR).

3.6. SAR study of JzTx-34 for $hNa_v1.1$ regulation

For this SAR study, we substituted each of the 29 non-cysteine residues of JzTx-34 by alanine, or by phenylalanine if an alanine was already present in the sequence, and examined their activities on $hNa_v1.1$ at maximally effective concentration (1 or 3 μM). We also tested a C-terminal amidated version of JzTx-34. As shown, among all 30 analogs produced, 8 of the mutations produced an almost complete loss of activity as judged by the lack of effect on hNa_v11 currents by the application of the analogs at 3 μM concentration (L^6A, L^{19}A, R^{22}A, P^{26}A, V^{30}A, W^{31}A, W^{33}A and T34A) (Fig. 6). An additional set of 8 other mutations (W^5A, H^{18}A, E^{20}A, K^{23}A, W^{25}A, Y^{27}A, H^{28}A, D^{32}A) also appeared to affect the ability of JzTx-34 to block channel inactivation as judged by the extent of inactivation slowing of $hNa_v1.1$ currents. Overall, these results provide a first indication that the pharmacophore of JzTx-34 mainly implicates C-terminal residues and a rather large interacting surface as judged by the number of essential residues. The JzTx-34 D^{14}A analog deserves a special mention, as it appears to promote a large sustained non-inactivating component, raising the interesting issue that some mutations may modulate the level at which channel inactivation kinetics is affected. To get a better grip on the effect of each of these variants on $hNa_v1.1$ currents, we evaluated dose-response curves for each of these analogs (Fig. 7). We examined the AUC ratio that quantifies the extent of current stimulation by the peptides and compared the curves to the one obtained with wild-type (WT) JzTx-34. Several conclusions can be reached based on these analyzes. First, we found that the E^4A mutation and the C-terminal amidation promote the inhibition of $hNa_v1.1$ inactivation kinetics by acting at lower concentrations than WT JzTx-34 (gain of function mutations). JzTx-34 E^4A increases the AUC ratio with EC_{50} values of 7.2 nM (maximum stimulation of 9.0-fold) compared to 42.9 nM for the WT peptide. In addition, JzTx-34-amide and JzTx-34 A17F lead to EC_{50} values of 27.1 and 33.0 nM, respectively (maximum stimulation of 12- and 8.6-fold). The gain of activity is therefore of 6.0-, 1.6- and 1.3-fold, respectively. The importance of C-terminal amidation in boosting toxin activity is classically observed [51]. In comparison, all other mutations were either neutral (A^1F and S^{10}A, EC_{50} = 60.2 nM; K^{11}A, 96.8 nM; A^{13}F, 52.4 nM; D^{14}A, 95.4 nM), induced mild loss of function (R^3A, EC_{50} = 241 nM; G^7A, 244 nM; G^8A, 105 nM; D^{12}A, 153 nM; V^{35}A, 192 nM), more severe (E^{20}A, 1174 nM; K^{24}A, 3285 nM; Y^{27}A, 1077 nM; T^{34}A, 1182 nM) or very severe (W^5A, L^6A, H^{18}A, L^{19}A, R^{22}A, K^{23}A, W^{25}A, P^{26}A, H^{28}A, V^{30}A, W^{31}A, D^{32}A, W^{33}A, all $EC_{50} > 3.3$ μM). This refined investigation points to 13 crucial residues for JzTx-34 activity and at least 4 more residues that alter the EC_{50} value by over 20-fold (E^{20}A, K^{24}A, Y^{27}A, T^{34}A). Based upon increase in AUC, the mutation JzTx-34 D^{14}A stands out as unusual, since the maximal stimulation of 14.3-fold is noticeably higher than the 9.8-fold for WT JzTx-34. Globally, the complexity emerging from the study of the functional pharmacophore of JzTx-34 requires a refined structural investigation for proper interpretation. We thus performed a complete set of additional NMR studies.

3.7. Structure of JzTx-34

The structure of JzTx-34 was determined by NMR (PDB access code 8CIQ). The chemical shift resonances are particularly dispersed attesting that JzTx-34 is well folded and indicating also that aromatic residues disturb the chemical shifts of surrounding residues. Note that the triad of tryptophan residues $W^5/W^{31}/W^{33}$ is responsible of out-of-range chemical shifts for a series of close protons, for example L^6(δ), H^{18}(β), L^{19}(α and δ) and W^{31} itself (β1 and indole). Other protons such as W^{25}(α), P^{26}(α) and H^{28}(β and δ) showed atypical chemical shifts too, influenced by Y^{27} and W^{25} itself. All the chemical shifts for ^{1}H, ^{15}N and ^{13}C were assigned except in a limited number of cases for $^{13}C_δ(K^{24})$, $^{13}C_α(W^{31})$ and $^{13}C_α(W^{33})$. They are accessible in the BioMagResBank resource (http://www.brmb.wisc.edu) with the following access codes: 34790 (wt JzTx-34), 34791 (H^{18}A), 34792 (E^{20}A), 34793 (W^{25}A), 34794 (W^{31}A) and 34795 (W^{33}A). NOE-derived restraints were progressively introduced in ARIA calculations until a final number of 781 NOE (Table 1). After only 4 runs of calculations the structures converged with a unique array of disulfide bridges, C^2–C^{16}, C^9–C^{21} and C^{15}–C^{29}, no violation of NOE > 0.3 Å and only 15 violations > 0.1 Å. The Ramachandran plot exhibits only 3.3 % of the (ϕ,ψ) angles in the disallowed regions, which mostly corresponds to the highly constrained adjacent residues C^{15}–C^{16} in the ICK motif, whereas 96 % of residues are in the most favored regions of the plot (Table 1).

The 3D structure of Wt JzTx-34 displays a distorted extended region around W^5 and L^6 (β1), two short β-strands, L^{19}–C^{21} (β2) and C^{29}-W^{31} (β3), forming a well-defined β-sheet, and is compacted by 3 disulfide bridges (C^2–C^{16}, C^9–C^{21} and C^{15}–C^{29}), thus forming the well-known ICK motif (Fig. 8a). A representation of the critical residues for the potency of JzTx-34 on inactivation of $hNa_v1.1$ shows the spatial distribution of all 16 important amino acid residues (W^5, L^6, H^{18}, L^{19}, E^{20}, R^{22}, K^{23}, K^{24}, W^{25}, Y^{27}, H^{28}, V^{30}, D^{32}, W^{31}, W^{33}, T^{34}), according to the SAR studies. All these residues are located on the same face of the peptide underlying the existence of an unusual large and complex pharmacophore for the interaction with $hNa_v1.1$ (Fig. 8b, left). The cases of L^{19} and V^{30} are peculiar since they are totally embedded in the core of the molecule, certainly pointing to an essential structural role. In an attempt to perfect our understanding of peptide folding and pharmacophore constitution, NMR spectra were acquired on ten JzTx-34 mutants. Depending on the positions of the residues mutated, the qualities of the NMR spectra varied considerably (Fig. S6). Good quality spectra were obtained for the

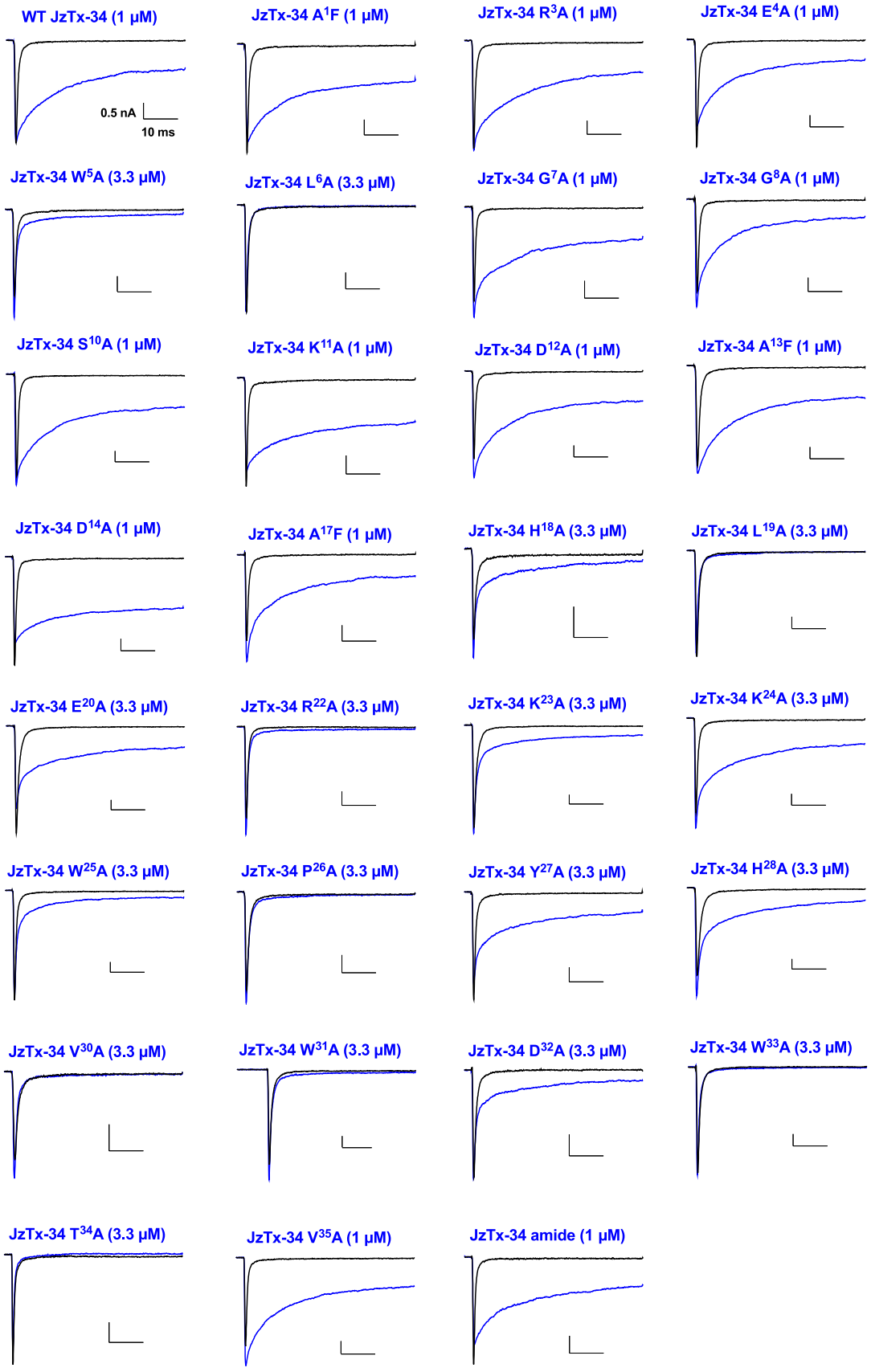

Fig. 6. Representative current traces of $hNa_v1.1$ before (black trace) and after (blue trace) application of 1 or 3.3 μM JzTz-34 analogs as specified. The highest concentration was used when almost no effect was detected at 1 μM. Holding potential was − 100 mV and test potential + 10 mV. Current amplitude scale bar is always 0.5 nA.

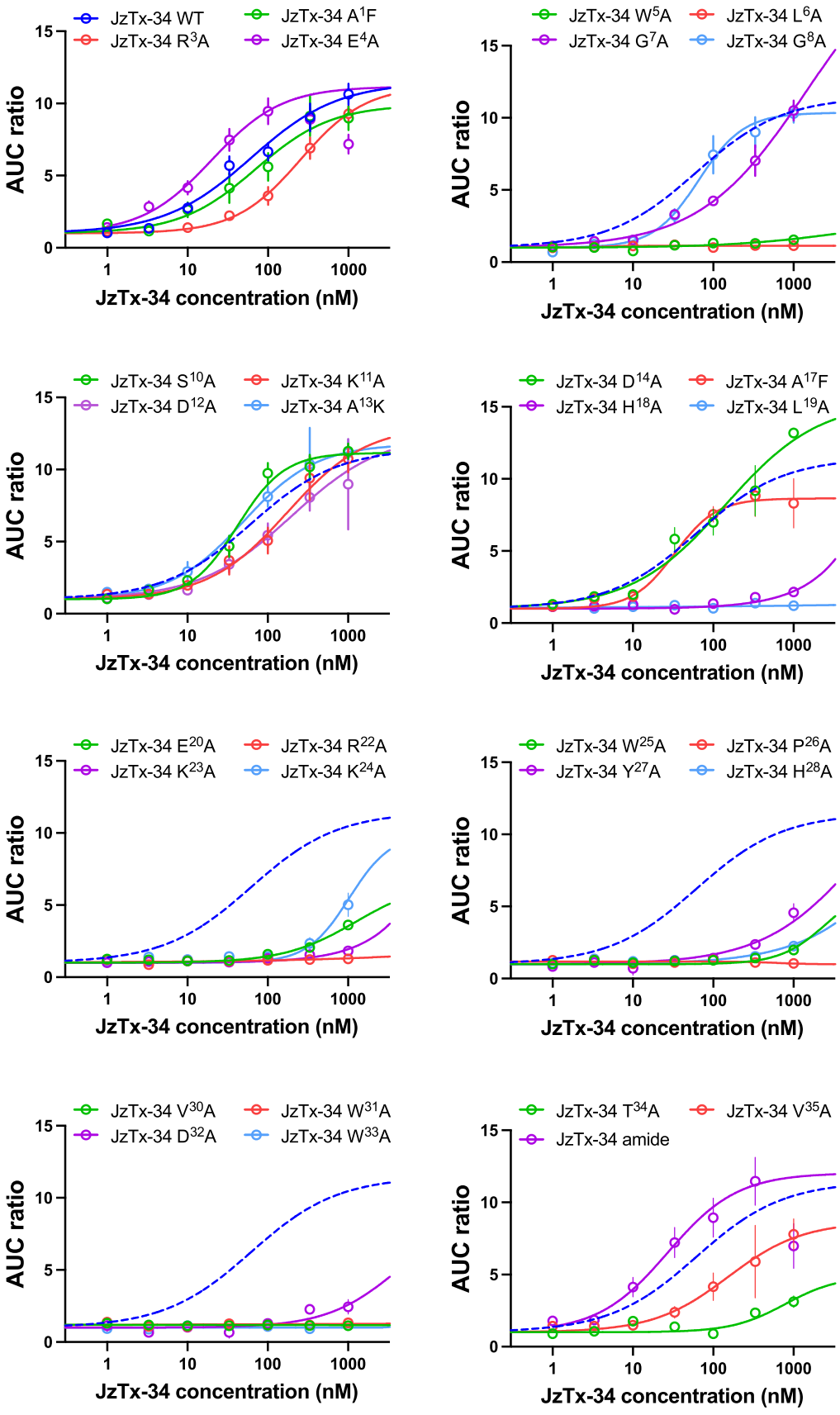

Fig. 7. Dose-response curves illustrating the impact of increasing JzTx-34 analog concentration on the AUC value, normalized to the control value before application of the peptide. 4–3 variants are shown on each figure to best illustrate the data. The dashed blue line is the dose-response curve of WT JzTx-34 shown for comparison. Note the higher AUC values reached by the $D^{14}A$ mutation. Note also that higher concentrations of JzTx-34 $E^{4}A$ (333 nM and 1 μM) lead to reduction in AUC stimulation probably because of peak current reduction possibly by binding onto another channel site.

Table 1
Experimental NMR data used for the calculations of Wt JzTx-34 solution structure, and final structural statistics for the ten representative models. a: values are given as mean ± standard deviation (n = 10).

NMR constraints	
Distance restraints	
Total NOE	781
Unambiguous	667
Ambiguous	114
Structural statistics (PDB code 8CIQ)	
Average violations per structure	
NOEs ≥ 0.3 Å	0
NOEs ≥ 0.1 Å	15
Rmsd (Å)	
Average pairwise rmsd (Å)	0.2
Ramachandran analysis	
Most favored region and allowed region	96 %
Generously allowed	0.7 %
Disallowed	3.3 %
Energies (kcal mol^{-1})^{a}	
Electrostatic	-1068 ± 23
Van der Walls	-311 ± 5
Total energy	-988 ± 30
Residual NOE energy	25 ± 5

H^{18}A, E^{20}A, W^{25}A, W^{31}A and W^{33}A mutants, which allowed the determination of high-resolution NMR structures (PDB codes 8CJP, 8CJQ, 8CJR, 8CJS and 8CJT, respectively). Poor quality spectra were obtained for the W^5A, L^6A, L^{19}A, R^{22}A and V^{30}A mutants indicating a folding deficiency, potentially linked to alteration in the disulfide-bridging patterns adopted by these analogs. As stated earlier, chemical synthesis of wt JzTx-34 was prone to produce two eluting peaks with the most hydrophobic one possessing the best activity. For its analogs, the relative percentage of each form of the peptide varied greatly with the nature of the mutation with W^5A, D^{12}A, D^{14}A, K^{23}A, P^{26}A, Y^{27}A, H^{28}A, V^{30}A and W^{31}A producing the greatest proportion of misfolded peptide (Fig. S7**).** On the opposite spectrum, L^6A, G^7A, G^8A, L^{19}A, E^{20}A, R^{22}A, W^{25}A and D^{32}A, produced a single peak. Clearly, we cannot conclude that all these analogs have the proper fold, but it emerges that some residues play key roles in orienting the folding of the peptide. The poor-quality spectra of the W^5A, L^6A, L^{19}A, R^{22}A and V^{30}A mutants do not allow us to unambiguously conclude that the residues at these positions are constitutive of the pharmacophore. These results are also coherent with the role of some of these residues in providing a hydrophobic core to the peptide. Hence, mutating these residues may destabilize this hydrophobic core and lead to misfolding by producing disruptive peptide conformations. It can be monitored for example on L^{19}A and V^{30}A mutants, which lead to poor quality NMR spectra. These two embedded residues face each other in the β-sheet (L^{19} in β2 and V^{30} in β3) that constitutes the core of JzTx-34. In contrast, the variants H^{18}A, E^{20}A, W^{25}A, W^{31}A and W^{33}A all yielded nice NMR spectra, fully coherent with a perfect preservation of the core structure of JzTx-34 (Fig. S6c). The NMR spectra of K^{23}, K^{24}, Y^{27}, H^{28}, D^{32}, and T^{34} have not been acquired, and these residues remain thus potential contributors of the pharmacophore.

How do these critical residues, constitutive of the pharmacophore or problematic for the folding, compare to the residues present in Hm1a at equivalent positions? Among the 16 residues influencing the $hNa_v1.1$ stimulation potency of JzTx-34 (and reported in red or orange in Fig. 8), H^{18}, L^{19}, R^{22}, W^{25}, Y^{27}, W^{31}, D^{32} and T^{34} are strictly conserved in Hm1a (Fig. S8). The structures of H^{18}, W^{25} and W^{31} attest that the 3D fold is perfectly maintained in these 3 mutants. The two residues forming the first β-strand of JzTx-34, namely W^5 and L^6, are replaced in Hm1a sequence by L and F, respectively (note that mutations at position 5 or 6 leads to poor NMR spectra). The ten conserved residues cover a large area of the pharmacophore, and the orientation of their sidechain are very well conserved in the 3D structures (Fig. S8). On the contrary, residues E^{20}, K^{23}, K^{24}, V^{30} and W^{33} (JzTx-34 numbering) are not conserved in Hm1a sequence, indicating that the interaction of Hm1a relies on a different pharmacophore for its interaction with $hNa_v1.1$ than JzTx-34. Among them, the 3D structures of E^{20}A and W^{33}A mutants have been checked. Finally, note that H^{28}, a crucial residue for JzTx-34 activity, is missing in Hm1a. Concerning folding issues, W^5 is substituted by L in Hm1a, L^6 by F, V^{30} by A, whereas L^{19} and R^{22} are conserved. Since mutations at these positions are problematic for JzTx-34 folding (they all provide poor NMR spectra), they may constitute lead positions to mutate Hm1a and improve its folding properties and synthesis yield.

4. Discussion

Using high-throughput screening systems, adapted to the complexity of spider venoms, that contain a high number of peptides with a large range of active concentrations, we were able to identify peptides active on $hNa_v1.1$. We rediscovered a known peptide, JzTx-34, whose effect on $hNa_v1.1$ was unnoticed [52]. A leading explanation for the differing finding is the species specificity of the peptides, as the previous studies used rat Na_v's and we have used the human orthologs. In addition, venom peptides possess a variable level of target promiscuity that explains why a peptide discovered earlier for its activity on a given target at a 100 nM to 1 μM affinity may very well be rediscovered for its activity on another target with a greater affinity.

Because of the severe medical consequences of neurological and cardiac diseases associated with a loss of activity of $Na_v1.1$, identifying new activating peptides for this channel type is an essential endeavor. The identification of JzTx-34 as an activator of $hNa_v1.1$ comes a few years after the identification of Hm1a, an interesting drug candidate for the treatment of Dravet syndrome [32]. Among other clear advantages linked to the use of Hm1a is the fact that this peptide is active on $hNa_v1.1$ target at 10-fold lower concentrations than JzTx-34. In addition, Hm1a produces similar modification of $Na_v1.1$ from both mice and humans, enabling proof-of-concept pharmacological studies. However, Hm1a is not devoid of defects that are inherent to its structure (difficult ICK fold to synthesize) and its sequence (limited selectivity with regard to the neuronal $Na_v1.2$ channel). As a matter of fact, the yield of production of Hm1a is extremely low and the active conformation with the correct assembly of its three disulfide bridges may easily be contaminated by variants with improper fold characteristics and hence peptide potency. In addition, the therapeutic window of the peptide is limited by its $Na_v1.2$ activating properties at low concentrations. It therefore does not meet the ideal criteria for a $Na_v1.1$ activating peptide: good yield of production and excellent selectivity for $Na_v1.1$ with regard to other neuronal Na_v channels ($Na_v1.2$ and $Na_v1.6$). Another worrying aspect of the peptide is that it is particularly difficult to understand which amino acid residue of the peptide is responsible for its activity on $hNa_v1.1$ because undertaking a SAR investigation on this hard to fold peptide would represent a daunting challenge. As such, since a clear visualization of Hm1a's pharmacophore is lacking, it is also difficult to engage in a process of synthesizing peptidomimetics that would circumvent the therapeutic limitations of Hm1a peptide. In some respects, JzTx-34 does not display better properties than Hm1a. We revealed the promiscuous nature of the peptide in Fig. 5. The peptide has activating properties on $hNa_v1.1$, $hNa_v1.3$ and $hNa_v1.6$ and mild ones on $hNa_v1.4$. JzTx-34 also blocks $hNa_v1.2$, $Na_v1.5$, $Na_v1.7$ and hERG channels, and mildly inhibits $hNa_v1.4$. In that respect, JzTx-34 is a remarkable model peptide for understanding the molecular basis of channel / peptide interactions as it has the capability to act as inhibitor, activator or even with mixed inhibitor / activator properties as on $hNa_v1.4$. If one is primarily interested in targeting the central nervous system, the activity revealed on both $hNa_v1.2$ and $hNa_v1.6$ is worrisome for a therapeutic use of JzTx-34 in Dravet syndrome, albeit no more worrisome than for Hm1a since there is between a 10-fold ($Na_v1.6$) and 25-fold ($Na_v1.2$) difference in channel selectivity for JzTx-34 in favor of $hNa_v1.1$. JzTx-34 has an advantage compared to Hm1a for three reasons: i) it will help identifying other peptides active on $hNa_v1.1$ on the basis of sequence similarities, ii) it is not hampered by its structure for high synthesis yield, and iii) a

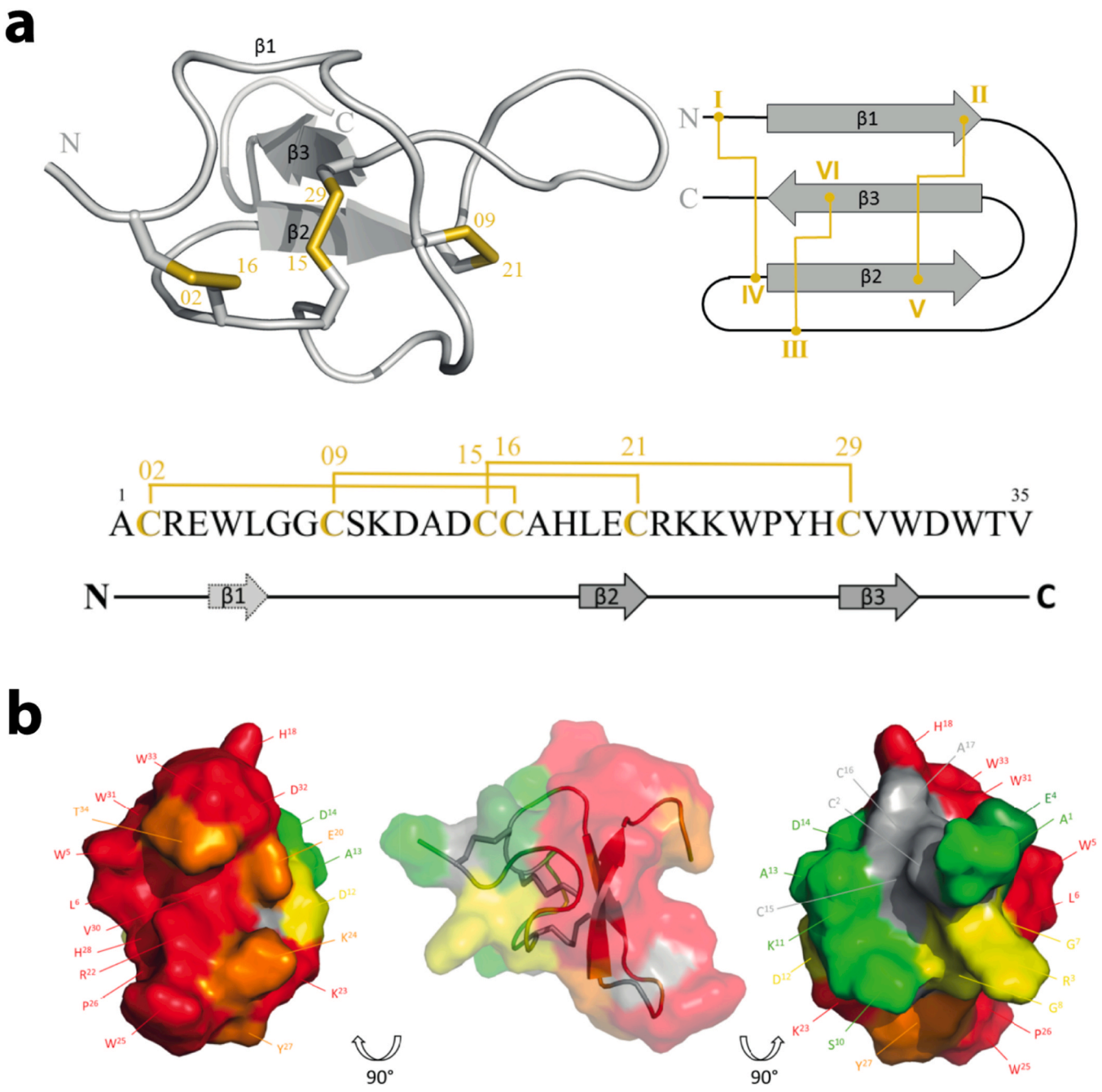

Fig. 8. (**a**) Top: ^{3}D NMR structure of JzTx-34 drawn with the PyMOL software (The PyMOL Molecular Graphics System, Version 2.0 Schrödinger, LLC). Grey arrows represent well defined β-strands, disulfide bridges are highlighted in yellow and cysteine residues are numbered. Bottom: primary structure of JzTx-34, with β-strands and disulfide bridges following the same color code. (**b**) Representation of peptide residues on the structure of JzTx-34 as a function of their importance for $hNa_v1.1$ stimulation potency. Essential and non-essential residues segregate two faces of the toxin, allowing the definition of a comprehensive set of residues important for the interaction with $hNa_v1.1$. Left: Amino acid residues W^5, L^6, H^{18}, L^{19}, E^{20}, R^{22}, K^{23}, K^{24}, W^{25}, Y^{27}, H^{28}, D^{32}, V^{30}, W^{31}, W^{33} and T^{34} are all essential for activity when mutated and a large fraction of them form the pharmacophore of JzTx-34 on $hNa_v1.1$ (residues in red and orange: $EC_{50} > 3.3$ μM and 1 μM, respectively). Right: On the opposite face, non-essential residues are R^3, G^7, G^8, D^{12}, V^{35} (yellow, 100 nM $< EC_{50} <$ 250 nM), A^1, S^{10}, K^{11}, A^{13}, D^{14} (light green, $EC_{50} <$ 100 nM), and E^4 (dark green, $EC_{50} <$ 40 nM). Middle: when the structure is shown from the side, it is obvious that the 3 disulfide bridges (grey sticks) are gathered on the side opposite the pharmacophore.

complete SAR investigation of this peptide could be undertaken. We had the opportunity to synthesize 30 single mutated analogs of JzTx-34 and the reference $Na_v1.1$ toxin activator Hm1a. From these efforts, we learned that JzTx-34 sequences easily tolerates alterations since most of the Ala-substituted analogs folded well. This was not the case of all positions however as we noticed some difficulties with several substitutions. These key problematic residues may help, in turn, the identification of those residues of Hm1a that pose problems for its chemical synthesis. Globally however, this effort led to the definition of a rather large pharmacophore, which was expected by the rather large repertoire of channels that can be modulated by this peptide. Interestingly, these efforts did not help define a form of minimal consensus pharmacophore of Hm1a, but that indicates that there must be several ways a peptide can produce $hNa_v1.1$ activation.

Ethics approval

All animal care and experimental procedures were performed in the animal facilities that have been accredited by the French Ministry of Agriculture. All animals were exposed to 12-h light/dark (light, 8:00 h to 20:00 h) in a thermostatically controlled room with free access to food and water. The experimental procedures were approved by the regional ethic committees (CEEA-006 Pays de la Loire and CEEA-036 Languedoc Roussillon, France) and authorized by the French Ministry of National Education (APAFIS #34541-2022010310194375 and 2017010310594939*)*, Higher Education and Research according to the Directive 2010/63/EU of the European Union.

Data deposition

The atomic coordinates of JzTx-34 and of 5 mutants having high quality NMR spectra, namely $H^{18}A$, $E^{20}A$, $W^{25}A$, $W^{31}A$ and $W^{33}A$, have been deposited in the Protein Data (https://www.wwpdb.org/) under the PDB access codes 8CIQ, 8CJP, 8CJQ, 8CJR, 8CJS ET 8CJT, respectively.

Funding

MDW thanks the Agence Nationale de la Recherche (ANR) for financial support (laboratory of excellence "Ion Channels, Science and Therapeutics" Grant no. ANR-11-LABX-0015 and Nav12RESCUE Grant no. ANR-21-CE18-0042). This work was also supported by the Fondation Leducq in the frame of its program of ERPT equipment support (purchase of the Syncropatch 384PE), by a grant "New Team" of the Région Pays de la Loire to **MDW** and by a European FEDER grant in support of the automated patch-clamp system.

CRediT authorship contribution statement

LL, **SDW**, **BOM** and **JM** performed automated patch clamp experiments and analyses. **HM** and **CL** performed the structural work. **CC** and **RB** synthesized the peptides. **KK**, **SL**, **JPJ** and **CC** performed the initial screening. **SS** and **MM** confirmed the effect of the peptide by manual patch clamp. **JDW** and FB tested JzTx-34 on Kv2.1 chimeras. **AT** followed the mice ECG after JzTx-34 *in vivo* injection. **SP** and **JT** tested the effect of the peptide on rat $Na_v1.1$. **MDW** managed the entire project and wrote the manuscript.

Declaration of Competing Interest

The authors declare the following financial interests/personal relationships which may be considered as potential competing interests: **CC** and **RB** are employee and CEO of Smartox Biotechnology, respectively. **MDW** is a founder and consultant of Smartox Biotechnology. **KK**, **SL** and **JPJ** are employees of Xenon Pharmaceuticals. **CC** is a past employee of Xenon Pharmaceuticals.

Data Availability

Data will be made available on request.

Appendix A. Supporting information

Supplementary data associated with this article can be found in the online version at doi:10.1016/j.biopha.2023.115173.

References

[1] C. Tian, K. Wang, W. Ke, H. Guo, Y. Shu, Molecular identity of axonal sodium channels in human cortical pyramidal cells, Front. Cell. Neurosci. 8 (2014) 297.
[2] I. Ogiwara, H. Miyamoto, N. Morita, N. Atapour, E. Mazaki, I. Inoue, T. Takeuchi, S. Itohara, Y. Yanagawa, K. Obata, T. Furuichi, T.K. Hensch, K. Yamakawa, Nav1.1 localizes to axons of parvalbumin-positive inhibitory interneurons: a circuit basis for epileptic seizures in mice carrying an Scn1a gene mutation, J. Neurosci. 27 (22) (2007) 5903–5914.
[3] Y. Almog, A. Mavashov, M. Brusel, M. Rubinstein, Functional investigation of a neuronal microcircuit in the CA1 area of the hippocampus reveals synaptic dysfunction in Dravet syndrome mice, Front. Mol. Neurosci. 15 (2022), 823640.
[4] F.H. Yu, M. Mantegazza, R.E. Westenbroek, C.A. Robbins, F. Kalume, K.A. Burton, W.J. Spain, G.S. McKnight, T. Scheuer, W.A. Catterall, Reduced sodium current in GABAergic interneurons in a mouse model of severe myoclonic epilepsy in infancy, Nat. Neurosci. 9 (9) (2006) 1142–1149.
[5] M. Mantegazza, S. Cestele, Pathophysiological mechanisms of migraine and epilepsy: similarities and differences, Neurosci. Lett. 667 (2018) 92–102.
[6] L.G. Sadleir, E.I. Mountier, D. Gill, S. Davis, C. Joshi, C. DeVile, M.A. Kurian, D.D. D. Study, S. Mandelstam, E. Wirrell, K.C. Nickels, H.R. Murali, G. Carvill, C. T. Myers, H.C. Mefford, I.E. Scheffer, Not all SCN1A epileptic encephalopathies are Dravet syndrome: early profound Thr226Met phenotype, Neurology 89 (10) (2017) 1035–1042.
[7] A. Brunklaus, T. Brunger, T. Feng, C. Fons, A. Lehikoinen, E. Panagiotakaki, M. A. Vintan, J. Symonds, J. Andrew, A. Arzimanoglou, S. Delima, J. Gallois, D. Hanrahan, G. Lesca, S. MacLeod, D. Marjanovic, A. McTague, N. Nunez-Enamorado, E. Perez-Palma, M. Scott Perry, K. Pysden, S.J. Russ-Hall, I.E. Scheffer, K. Sully, S. Syrbe, U. Vaher, M. Velayutham, J. Vogt, S. Weiss, E. Wirrell, S. M. Zuberi, D. Lal, R.S. Moller, M. Mantegazza, S. Cestele, The gain of function SCN1A disorder spectrum: novel epilepsy phenotypes and therapeutic implications, Brain 145 (11) (2022) 3816–3831.
[8] S. Matricardi, S. Cestele, M. Trivisano, B. Kassabian, N. Leroudier, R. Vittorini, M. Nosadini, E. Cesaroni, S. Siliquini, C. Marinaccio, F. Longaretti, B. Podesta, F. F. Operto, C. Luisi, S. Sartori, C. Boniver, N. Specchio, F. Vigevano, C. Marini, M. Mantegazza, Gain of function SCN1A disease-causing variants: expanding the phenotypic spectrum and functional studies guiding the choice of effective antiseizure medication, Epilepsia (2023).
[9] C. Dravet, The core Dravet syndrome phenotype, Epilepsia 52 Suppl 2 (2011) 3–9.
[10] M. Mantegazza, S. Cestele, W.A. Catterall, Sodium channelopathies of skeletal muscle and brain, Physiol. Rev. 101 (4) (2021) 1633–1689.
[11] C. Depienne, O. Trouillard, C. Saint-Martin, I. Gourfinkel-An, D. Bouteiller, W. Carpentier, B. Keren, B. Abert, A. Gautier, S. Baulac, A. Arzimanoglou, C. Cazeneuve, R. Nabbout, E. LeGuern, Spectrum of SCN1A gene mutations associated with Dravet syndrome: analysis of 333 patients, J. Med. Genet. 46 (3) (2009) 183–191.
[12] Y.W. Wu, J. Sullivan, S.S. McDaniel, M.H. Meisler, E.M. Walsh, S.X. Li, M. W. Kuzniewicz, Incidence of Dravet syndrome in a US population, Pediatrics 136 (5) (2015) e1310–e1315.
[13] F. Guzzetta, Cognitive and behavioral characteristics of children with Dravet syndrome: an overview, Epilepsia 52 Suppl 2 (2011) 35–38.
[14] A. Escayg, A.L. Goldin, Sodium channel SCN1A and epilepsy: mutations and mechanisms, Epilepsia 51 (9) (2010) 1650–1658.
[15] S. Ito, I. Ogiwara, K. Yamada, H. Miyamoto, T.K. Hensch, M. Osawa, K. Yamakawa, Mouse with Nav1.1 haploinsufficiency, a model for Dravet syndrome, exhibits lowered sociability and learning impairment, Neurobiol. Dis. 49 (2013) 29–40.
[16] T. Tatsukawa, I. Ogiwara, E. Mazaki, A. Shimohata, K. Yamakawa, Impairments in social novelty recognition and spatial memory in mice with conditional deletion of Scn1a in parvalbumin-expressing cells, Neurobiol. Dis. 112 (2018) 24–34.
[17] J. Kearney, Sudden unexpected death in dravet syndrome, Epilepsy Curr. 13 (6) (2013) 264–265.
[18] C.R. Frasier, H. Zhang, J. Offord, L.T. Dang, D.S. Auerbach, H. Shi, C. Chen, A. M. Goldman, L.L. Eckhardt, V.J. Bezzerides, J.M. Parent, L.L. Isom, Channelopathy as a SUDEP biomarker in Dravet syndrome patient-derived cardiac myocytes, Stem Cell Rep. 11 (3) (2018) 626–634.
[19] R. Surges, R.D. Thijs, H.L. Tan, J.W. Sander, Sudden unexpected death in epilepsy: risk factors and potential pathomechanisms, Nat. Rev. Neurol. 5 (9) (2009) 492–504.
[20] M.S. Cooper, A. McIntosh, D.E. Crompton, J.M. McMahon, A. Schneider, K. Farrell, V. Ganesan, D. Gill, S. Kivity, T. Lerman-Sagie, A. McLellan, J. Pelekanos, V. Ramesh, L. Sadleir, E. Wirrell, I.E. Scheffer, Mortality in Dravet syndrome, Epilepsy Res. 128 (2016) 43–47.
[21] S. Han, C. Tai, R.E. Westenbroek, F.H. Yu, C.S. Cheah, G.B. Potter, J.L. Rubenstein, T. Scheuer, H.O. de la Iglesia, W.A. Catterall, Autistic-like behaviour in Scn1a+/- mice and rescue by enhanced GABA-mediated neurotransmission, Nature 489 (7416) (2012) 385–390.
[22] L. Verret, E.O. Mann, G.B. Hang, A.M. Barth, I. Cobos, K. Ho, N. Devidze, E. Masliah, A.C. Kreitzer, I. Mody, L. Mucke, J.J. Palop, Inhibitory interneuron deficit links altered network activity and cognitive dysfunction in Alzheimer model, Cell 149 (3) (2012) 708–721.
[23] K.H. Lim, Z. Han, H.Y. Jeon, J. Kach, E. Jing, S. Weyn-Vanhentenryck, M. Downs, A. Corrionero, R. Oh, J. Scharner, A. Venkatesh, S. Ji, G. Liau, B. Ticho, H. Nash, I. Aznarez, Antisense oligonucleotide modulation of non-productive alternative splicing upregulates gene expression, Nat. Commun. 11 (1) (2020) 3501.
[24] Z. Han, C. Chen, A. Christiansen, S. Ji, Q. Lin, C. Anumonwo, C. Liu, S.C. Leiser, Meena, I. Aznarez, G. Liau, L.L. Isom, Antisense oligonucleotides increase Scn1a expression and reduce seizures and SUDEP incidence in a mouse model of Dravet syndrome, Sci. Transl. Med. 12 (558) (2020).
[25] A.M. Glazer, Y. Wada, B. Li, A. Muhammad, O.R. Kalash, M.J. O'Neill, T. Shields, L. Hall, L. Short, M.A. Blair, B.M. Kroncke, J.A. Capra, D.M. Roden, High-throughput reclassification of SCN5A variants, Am. J. Hum. Genet. 107 (1) (2020) 111–123.

[26] G. Colasante, G. Lignani, S. Brusco, C. Di Berardino, J. Carpenter, S. Giannelli, N. Valassina, S. Bido, R. Ricci, V. Castoldi, S. Marenna, T. Church, L. Massimino, G. Morabito, F. Benfenati, S. Schorge, L. Leocani, D.M. Kullmann, V. Broccoli, dCas9-based Scn1a gene activation restores inhibitory interneuron excitability and attenuates seizures in Dravet syndrome mice, Mol. Ther.: J. Am. Soc. Gene Ther. 28 (1) (2020) 235–253.
[27] J. Perez, C. Chiron, C. Musial, E. Rey, H. Blehaut, P. d'Athis, J. Vincent, O. Dulac, Stiripentol: efficacy and tolerability in children with epilepsy, Epilepsia 40 (11) (1999) 1618–1626.
[28] O. Devinsky, J.H. Cross, S. Wright, Trial of cannabidiol for drug-resistant seizures in the Dravet syndrome, N. Engl. J. Med. 377 (7) (2017) 699–700.
[29] C.Y. Chow, Y.K.Y. Chin, L. Ma, E.A.B. Undheim, V. Herzig, G.F. King, A selective NaV1.1 activator with potential for treatment of Dravet syndrome epilepsy, Biochem. Pharm. 181 (2020), 113991.
[30] J.D. Osteen, V. Herzig, J. Gilchrist, J.J. Emrick, C. Zhang, X. Wang, J. Castro, S. Garcia-Caraballo, L. Grundy, G.Y. Rychkov, A.D. Weyer, Z. Dekan, E. A. Undheim, P. Alewood, C.L. Stucky, S.M. Brierley, A.I. Basbaum, F. Bosmans, G. F. King, D. Julius, Selective spider toxins reveal a role for the Nav1.1 channel in mechanical pain, Nature 534 (7608) (2016) 494–499.
[31] J.D. Osteen, K. Sampson, V. Iyer, D. Julius, F. Bosmans, Pharmacology of the Nav1.1 domain IV voltage sensor reveals coupling between inactivation gating processes, Proc. Natl. Acad. Sci. USA 114 (26) (2017) 6836–6841.
[32] K.L. Richards, C.J. Milligan, R.J. Richardson, N. Jancovski, M. Grunnet, L. H. Jacobson, E.A.B. Undheim, M. Mobli, C.Y. Chow, V. Herzig, A. Csoti, G. Panyi, C.A. Reid, G.F. King, S. Petrou, Selective NaV1.1 activation rescues Dravet syndrome mice from seizures and premature death, Proc. Natl. Acad. Sci. USA 115 (34) (2018) E8077–E8085.
[33] O. Chever, S. Zerimech, P. Scalmani, L. Lemaire, L. Pizzamiglio, A. Loucif, M. Ayrault, M. Krupa, M. Desroches, F. Duprat, I. Lena, S. Cestele, M. Mantegazza, Initiation of migraine-related cortical spreading depolarization by hyperactivity of GABAergic neurons and NaV1.1 channels, J. Clin. Invest. 131 (21) (2021).
[34] W.F. Vranken, W. Boucher, T.J. Stevens, R.H. Fogh, A. Pajon, M. Llinas, E.L. Ulrich, J.L. Markley, J. Ionides, E.D. Laue, The CCPN data model for NMR spectroscopy: development of a software pipeline, Proteins 59 (4) (2005) 687–696.
[35] W. Rieping, M. Habeck, B. Bardiaux, A. Bernard, T.E. Malliavin, M. Nilges, ARIA2: automated NOE assignment and data integration in NMR structure calculation, Bioinformatics 23 (3) (2007) 381–382.
[36] R.A. Laskowski, J.A. Rullmannn, M.W. MacArthur, R. Kaptein, J.M. Thornton, AQUA and PROCHECK NMR: programs for checking the quality of protein structures solved by NMR, J. Biomol. NMR 8 (4) (1996) 477–486.
[37] J. Chen, Y. Zhang, M. Rong, L. Zhao, L. Jiang, D. Zhang, M. Wang, Y. Xiao, S. Liang, Expression and characterization of jingzhaotoxin-34, a novel neurotoxin from the venom of the tarantula Chilobrachys jingzhao, Peptides 30 (6) (2009) 1042–1048.
[38] X. Dehong, W. Wenmei, H. Siqin, Z. Peng, W. Xianchun, Z. Xiongzhi, Effects of JZTX-V on the wild type Kv4.3 expressed in HEK293T and molecular determinants in the voltage-sensing domains of Kv4.3 interacting with JZTX-V, Channels 16 (1) (2022) 72–83.
[39] M. Deng, L. Jiang, X. Luo, H. Tao, S. Liang, Jingzhaotoxin-X, a gating modifier of Kv4.2 and Kv4.3 potassium channels purified from the venom of the Chinese tarantula Chilobrachys jingzhao, J. Venom. Anim. Toxins Incl. Trop. Dis. 26 (2020), e20190043.
[40] Y. Huang, X. Zhou, C. Tang, Y. Zhang, H. Tao, P. Chen, Z. Liu, Molecular basis of the inhibition of the fast inactivation of voltage-gated sodium channel Nav1.5 by tarantula toxin Jingzhaotoxin-II, Peptides 68 (2015) 175–182.
[41] C. Tang, X. Zhou, Y. Huang, Y. Zhang, Z. Hu, M. Wang, P. Chen, Z. Liu, S. Liang, The tarantula toxin jingzhaotoxin-XI (kappa-theraphotoxin-Cj1a) regulates the activation and inactivation of the voltage-gated sodium channel Nav1.5, Toxicon 92 (2014) 6–13.
[42] H. Tao, J.J. Chen, Y.C. Xiao, Y.Y. Wu, H.B. Su, D. Li, H.Y. Wang, M.C. Deng, M. C. Wang, Z.H. Liu, S.P. Liang, Analysis of the interaction of tarantula toxin Jingzhaotoxin-III (beta-TRTX-Cj1alpha) with the voltage sensor of Kv2.1 uncovers the molecular basis for cross-activities on Kv2.1 and Nav1.5 channels, Biochemistry 52 (42) (2013) 7439–7448.
[43] H. Tao, X. Chen, M. Deng, Y. Xiao, Y. Wu, Z. Liu, S. Zhou, Y. He, S. Liang, Interaction site for the inhibition of tarantula Jingzhaotoxin-XI on voltage-gated potassium channel Kv2.1, Toxicon 124 (2016) 8–14.
[44] Y. Wang, Z. Luo, S. Lei, S. Li, X. Li, C. Yuan, Effects and mechanism of gating modifier spider toxins on the hERG channel, Toxicon 189 (2021) 56–64.
[45] P. Wei, C. Xu, Q. Wu, L. Huang, S. Liang, C. Yuan, Jingzhaotoxin-35, a novel gating-modifier toxin targeting both Nav1.5 and Kv2.1 channels, Toxicon 92 (2014) 90–96.
[46] X.Z. Zeng, Q. Zhu, S.P. Liang, Sequence-specific assignment of ^{1}H NMR resonance and determination of the secondary structure of Jingzhaotoxin-I, Acta Biochim. Biophys. Sin. 37 (8) (2005) 567–572.
[47] J. Zhang, D. Tang, S. Liu, H. Hu, S. Liang, C. Tang, Z. Liu, Purification and characterization of JZTx-14, a potent antagonist of mammalian and prokaryotic voltage-gated sodium channels, Toxins 10 (10) (2018).
[48] X. Zeng, P. Li, B. Chen, J. Huang, R. Lai, J. Liu, M. Rong, Selective closed-state Nav1.7 blocker JZTX-34 exhibits analgesic effects against pain, Toxins 10 (2) (2018).
[49] J. Gilchrist, F. Bosmans, Using voltage-sensor toxins and their molecular targets to investigate Na(V) 1.8 gating, J. Physiol. 596 (10) (2018) 1863–1872.
[50] J. Montnach, L.A. Blomer, L. Lopez, L. Filipis, H. Meudal, A. Lafoux, S. Nicolas, D. Chu, C. Caumes, R. Beroud, C. Jopling, F. Bosmans, C. Huchet, C. Landon, M. Canepari, De, M. Waard, In vivo spatiotemporal control of voltage-gated ion channels by using photoactivatable peptidic toxins, Nat. Commun. 13 (1) (2022) 417.
[51] L. Lopez, J. Montnach, B. Oliveira-Mendes, K. Khakh, B. Thomas, S. Lin, C. Caumes, S. Wesolowski, S. Nicolas, D. Servent, C. Cohen, R. Beroud, E. Benoit, M. De Waard, Synthetic analogues of Huwentoxin-IV spider peptide with altered human Na(V) 1.7/Na(V)1.6 selectivity ratios, Front. Cell Dev. Biol. 9 (2021), 798588.
[52] C.Y. Chow, B. Cristofori-Armstrong, E.A. Undheim, G.F. King, L.D. Rash, Three peptide modulators of the human voltage-gated sodium channel 1.7, an important analgesic target, from the venom of an Australian Tarantula, Toxins 7 (7) (2015) 2494–2513.